

# IMPLICIT-EXPLICIT MULTIRATE INFINITESIMAL METHODS \*

RUJEKO CHINOMONA<sup>†</sup> AND DANIEL R. REYNOLDS<sup>†</sup>

**Abstract.** This work focuses on the development of a new class of high-order accurate methods for multirate time integration of systems of ordinary differential equations. Unlike other recent work in this area, the proposed methods support mixed implicit-explicit (IMEX) treatment of the slow time scale. In addition to allowing this flexibility at the slow time scale, the proposed methods utilize a so-called ‘infinitesimal’ formulation for the fast time scale through definition of a sequence of modified ‘fast’ initial-value problems, that may be solved using any viable solver. We name the proposed class as implicit-explicit multirate infinitesimal (IMEX-MRI) methods. In addition to defining these methods, we prove that they may be viewed as specific instances of generalized-structure additive Runge–Kutta (GARK) methods [35], and derive a set of order conditions on the IMEX-MRI coefficients to guarantee both third and fourth order accuracy for the overall multirate method. Additionally, we provide three specific IMEX-MRI methods, two of order three and one of order four. We conclude with numerical simulations demonstrating their predicted convergence rates on two multirate test problems, and compare their efficiency against legacy IMEX multirate methods.

**Key words.** multirate time integration, implicit-explicit methods, multirate infinitesimal step, multiple time stepping, ordinary differential equations

**AMS subject classifications.** 65L04, 65L05, 65L06, 65L20

**1. Introduction.** In recent years, there has been a renewed interest in time integration methods, most notably those that allow both high accuracy and increased flexibility with regard to how various components of the problem are treated. These methods range from those that apply a uniform time step size for all components of a problem but vary the algorithms used on individual terms, to ‘multirate’ methods that evolve separate solution components using different step sizes.

Methods in the former category have been introduced primarily to handle problems that couple stiff and nonstiff processes. Here, instead of applying a fully implicit or fully explicit treatment, that would be ideally suited to only the stiff or nonstiff components of the problem, respectively, these approaches allow more robust implicit solvers to be applied to the stiff components, leaving the remaining nonstiff (and frequently nonlinear) components to be treated explicitly. Various techniques within this category include mixed implicit-explicit (IMEX) additive Runge–Kutta methods [2, 1, 11, 12, 19, 20, 35], exponential Runge–Kutta (ExpRK) and exponential Rosenbrock (ExpRB) methods [18, 24, 25, 28, 42, 41] and general linear methods (GLM) [6, 5, 31, 45, 44].

Multirate methods, on the other hand, evolve separate solution components or dynamical processes using entirely different time step sizes. These frequently arise due to ‘multiphysics’ problems wherein separate physical processes evolve on disparate time scales. Either due to stability or accuracy considerations the ‘fast’ processes must be evolved with small step sizes, but due to their computational cost the ‘slow’ processes are evolved using sometimes much larger time steps. While simplistic low-order ‘subcycling’ approaches have been employed in computational simulations for

---

\*Submitted to the editors DATE.

**Funding:** Support for this work was provided by the U.S. Department of Energy, Office of Science project “Frameworks, Algorithms and Scalable Technologies for Mathematics (FASTMath),” under Lawrence Livermore National Laboratory subcontract B626484.

<sup>†</sup>Department of Mathematics, Southern Methodist University, Dallas, TX (rchinomona@smu.edu, reynolds@smu.edu).

decades, research into higher-order approaches has seen dramatic recent advances [3, 10, 14, 15, 23, 30, 29, 33, 36, 37, 39, 43].

In this paper we introduce a hybrid of two of the above techniques: IMEX Runge–Kutta and multirate methods. While the large majority of recent research on multirate methods has focused on the two-way, additively partitioned initial-value problem (IVP) combining a fast  $\{F\}$  and a slow  $\{S\}$  process,

$$(1.1) \quad y' = f(t, y) = f^{\{F\}}(t, y) + f^{\{S\}}(t, y), \quad y(t_0) = y_0, \quad t \in [t_0, t_f],$$

we focus on problems that further break down the slow portion into stiff  $\{I\}$  and nonstiff  $\{E\}$  components. Thus we consider the three-way additively partitioned IVP:

$$(1.2) \quad y' = f^{\{I\}}(t, y) + f^{\{E\}}(t, y) + f^{\{F\}}(t, y), \quad y(t_0) = y_0, \quad t \in [t_0, t_f].$$

Of the various approaches for multirate integration, we focus on those that are agnostic as to the precise methods applied to the fast dynamics. These are based on ‘infinitesimal’ formulations, including the seminal work on multirate infinitesimal step (MIS) methods [36, 43] and their more recent extensions to higher temporal order [3, 23, 30, 33, 39]. In such formulations, the fast dynamics are assumed to be solved ‘exactly’, typically through evolution of a sequence of modified fast IVPs,

$$v'(\theta) = f^{\{F\}}(\theta, v) + g(\theta), \quad v(\theta_0) = v_0, \quad \theta \in [\theta_0, \theta_f],$$

where the forcing function  $g(\theta)$  is determined by the multirate method to incorporate information from  $f^{\{S\}}$ . In practice, these fast IVPs are solved using another numerical method with smaller step size, which in turn could employ further decompositions via an IMEX, ExpRK, ExpRB, GLM, or multirate approach.

To our knowledge, there exist only two multirate schemes that simultaneously allow IMEX treatment of the slow dynamics and *arbitrary* treatment of the fast dynamics, both of which have low accuracy and have been shown to demonstrate poor stability [13, 32]. The first of these is the standard first order ‘Lie–Trotter’ splitting that performs the time step  $y_{n-1} \rightarrow y_n$  (here  $y_n \approx y(t)$  and  $t_n - t_{n-1} = H$ ) [27] via the algorithm:

$$(1.3) \quad \begin{aligned} y_n^{(1)} &= y_{n-1} + H f^{\{E\}}(t_{n-1}, y_{n-1}), \\ y_n^{(2)} &= y_n^{(1)} + H f^{\{I\}}(t_n, y_n^{(2)}), \\ \text{Solve } &\begin{cases} v(0) = y_n^{(2)}, \\ v'(\theta) = f^{\{F\}}(t_{n-1} + \theta, v), \text{ for } \theta \in [0, H], \end{cases} \\ y_n &= v(H). \end{aligned}$$

The second is a variant of the second order ‘Strang’ (or ‘Strang–Marchuk’) splitting formulation [26, 40],

$$(1.4) \quad \begin{aligned} y_n^{(1)} &= y_{n-1} + \frac{H}{4} f^{\{E\}}(t_{n-1}, y_{n-1}) \\ &\quad + \frac{H}{4} f^{\{E\}}\left(t_{n-1} + \frac{H}{2}, y_{n-1} + \frac{H}{2} f^{\{E\}}(t_{n-1}, y_{n-1})\right), \\ y_n^{(2)} &= y_n^{(1)} + \frac{H}{4} f^{\{I\}}(t_{n-1}, y_n^{(1)}) + \frac{H}{4} f^{\{I\}}\left(t_{n-1} + \frac{H}{2}, y_n^{(2)}\right), \\ \text{Solve } &\begin{cases} v(0) = y_n^{(2)}, \\ v'(\theta) = f^{\{F\}}(t_n + \theta, v), \text{ for } \theta \in [0, H], \end{cases} \end{aligned}$$

$$\begin{aligned}
 y_n^{(3)} &= v(H), \\
 y_n^{(4)} &= y_n^{(3)} + \frac{H}{4} f^{\{I\}} \left( t_{n-1} + \frac{H}{2}, y_n^{(3)} \right) + \frac{H}{4} f^{\{I\}} \left( t_n, y_n^{(4)} \right), \\
 y_n &= y_n^{(4)} + \frac{H}{4} f^{\{E\}} \left( t_{n-1} + \frac{H}{2}, y_n^{(4)} \right) \\
 &\quad + \frac{H}{4} f^{\{E\}} \left( t_n, y_n^{(4)} + \frac{H}{2} f^{\{E\}} \left( t_{n-1} + \frac{H}{2}, y_n^{(4)} \right) \right).
 \end{aligned}$$

We note that here, the updates  $y_{n-1} \rightarrow y_n^{(1)}$  and  $y_n^{(4)} \rightarrow y_n$  correspond to using the explicit Heun method for a half time-step each, while the updates  $y_n^{(1)} \rightarrow y_n^{(2)}$  and  $y_n^{(3)} \rightarrow y_n^{(4)}$  correspond to using the implicit trapezoid rule for a half time-step each. However to our knowledge, there do not exist multirate methods allowing IMEX treatment of the slow time scale that have order of accuracy three or higher. The purpose of this paper is to address this need, through proposal of a new class of *implicit-explicit multirate infinitesimal* (IMEX-MRI) methods for problems of the form (1.2), including derivation of order conditions up to fourth order, and numerical tests to demonstrate the benefit of such methods over the legacy approaches (1.3) and (1.4).

**2. Implicit-Explicit Multirate Infinitesimal Methods.** We base our proposed methods off of the MRI-GARK class of two-component multirate methods [34]. Just as those methods begin with an explicit or diagonally-implicit Runge-Kutta method for the slow time scale, we start with an IMEX additive Runge-Kutta scheme (IMEX-ARK) of order  $q$  and having  $\tilde{s}^{\{S\}}$  stages. These methods are characterized by a pair of Butcher tables:

$$\begin{array}{c|c} c^{\{E\}} & A^{\{E\}} \\ \hline 1 & b^{\{E\}T} \end{array} \quad \begin{array}{c|c} c^{\{I\}} & A^{\{I\}} \\ \hline 1 & b^{\{I\}T} \end{array}$$

In construction of IMEX-MRI methods, we place three additional restrictions on the base IMEX-ARK method: (a) the tables are ‘‘internally consistent,’’ (i.e.,  $c^{\{E\}} = c^{\{I\}} := c^{\{S\}}$ ), (b) the tables have explicit slow first stage (i.e.,  $c_1^{\{S\}} = 0$ ), and (c) the tables have non-decreasing abscissae (i.e.,  $c_1^{\{S\}} \leq c_2^{\{S\}} \leq \dots \leq c_{\tilde{s}^{\{S\}}}^{\{S\}}$ ). To reduce complexity in our analyses we follow [30, 34] and write the base IMEX-ARK method in stiffly accurate form, i.e., the last row of  $A^{\{E\}}$  and  $A^{\{I\}}$  equal  $b^{\{E\}T}$  and  $b^{\{I\}T}$ , respectively. We note that for methods that do not satisfy this requirement in simplest form, they may easily be converted to the stiffly accurate form by padding  $c$  and  $A$  with 1 and  $b^T$ , respectively:

$$\begin{array}{c|c|c} c^{\{S\}} & A^{\{E\}} & A^{\{I\}} \\ \hline 1 & b^{\{E\}T} & b^{\{I\}T} \end{array} \rightarrow \begin{array}{c|c|c|c|c} c^{\{S\}} & A^{\{E\}} & 0^{\{S\}} & A^{\{I\}} & 0^{\{S\}} \\ \hline 1 & b^{\{E\}T} & 0 & b^{\{I\}T} & 0 \\ \hline 1 & b^{\{E\}T} & 0 & b^{\{I\}T} & 0 \end{array}$$

where  $0^{\{S\}} \in \mathbb{R}^{\tilde{s}^{\{S\}}}$ . Thus for the remainder of this paper, we let  $A^{\{E,E\}}, A^{\{I,I\}} \in \mathbb{R}^{s^{\{S\}} \times s^{\{S\}}}$  be the stiffly-accurate versions of the IMEX-ARK Butcher tables  $A^{\{E\}}$  and  $A^{\{I\}}$ , respectively. We note that this extension of the tables to include the row of  $b$  coefficients does not affect the order conditions of the original IMEX-ARK table, and thus all order conditions satisfied by the original IMEX-ARK tables remain unchanged. Based on the above assumption of sorted abscissae, the increments between

consecutive stages are given by

$$(2.1) \quad \Delta c_i^{\{S\}} := \begin{cases} 0, & i = 1, \\ c_i^{\{S\}} - c_{i-1}^{\{S\}} \geq 0, & i = 2, \dots, s^{\{S\}}. \end{cases}$$

DEFINITION 2.1 (IMEX-MRI methods for additively partitioned systems). *The following algorithm defines one step from  $t_n$  to  $t_n + H$  of an IMEX-MRI scheme for the problem (1.2):*

$$(2.2a) \quad \text{Let : } Y_1^{\{S\}} := y_n$$

$$(2.2b) \quad \text{For } i = 2, \dots, s^{\{S\}} :$$

$$(2.2c) \quad \begin{cases} \text{Let: } v(0) := Y_{i-1}^{\{S\}} \text{ and } T_{i-1} := t_n + c_{i-1}^{\{S\}}H, \\ \text{Solve: } v'(\theta) = \Delta c_i^{\{S\}} f^{\{F\}} \left( T_{i-1} + \Delta c_i^{\{S\}}\theta, v(\theta) \right) \\ \quad + \sum_{j=1}^i \gamma_{i,j} \left( \frac{\theta}{H} \right) f_j^{\{I\}} + \sum_{j=1}^{i-1} \omega_{i,j} \left( \frac{\theta}{H} \right) f_j^{\{E\}}, \text{ for } \theta \in [0, H], \\ \text{Let: } Y_i^{\{S\}} := v(H), \end{cases}$$

$$(2.2d) \quad y_{n+1} = Y_{s^{\{S\}}}^{\{S\}}.$$

where  $f_j^{\{I\}} := f^{\{I\}} \left( t_n + c_j^{\{S\}}H, Y_j^{\{S\}} \right)$  and  $f_j^{\{E\}} := f^{\{E\}} \left( t_n + c_j^{\{S\}}H, Y_j^{\{S\}} \right)$ .

DEFINITION 2.2 (Slow tendency coefficients). *The coefficients  $\gamma_{i,j}$  and  $\omega_{i,j}$  from equation (2.2c) are polynomials in time that dictate the couplings from the slow to the fast time scale. As in [34],  $\gamma_{i,j}$  are defined as:*

$$(2.3) \quad \gamma_{i,j}(\tau) := \sum_{k \geq 0} \gamma_{i,j}^{\{k\}} \tau^k, \quad \tilde{\gamma}_{i,j}(t) := \int_0^t \gamma_{i,j}(\tau) d\tau = \sum_{k \geq 0} \gamma_{i,j}^{\{k\}} \frac{t^{k+1}}{k+1}, \quad \bar{\gamma}_{i,j} := \tilde{\gamma}_{i,j}(1),$$

and the coefficients  $\omega_{i,j}(\tau)$  are defined similarly. Through the remainder of the paper we refer to  $\Gamma^{\{k\}}, \Omega^{\{k\}}, \bar{\Gamma}$  and  $\bar{\Omega}$  as the matrices containing the coefficients  $\{\gamma_{i,j}^{\{k\}}\}, \{\omega_{i,j}^{\{k\}}\}, \{\bar{\gamma}_{i,j}\}$  and  $\{\bar{\omega}_{i,j}\}$ , respectively. We note that Definitions 2.1 and 2.2 differ slightly from those in [34], in that we consider these tendency coefficients to be organized into  $s^{\{S\}} \times s^{\{S\}}$  matrices having first row identically zero.

We note that a consistency condition for these tendency coefficients arises from application of (2.2) to a problem with no fast time scale. Supposing that  $f^{\{F\}} = 0$ , then for  $i = 2, \dots, s^{\{S\}}$ , (2.2c) becomes

$$\begin{aligned} Y_i^{\{S\}} &= Y_{i-1}^{\{S\}} + H \sum_{j=1}^i \bar{\gamma}_{i,j} f_j^{\{I\}} + H \sum_{j=1}^{i-1} \bar{\omega}_{i,j} f_j^{\{E\}} \\ &= y_n + H \sum_{l=1}^i \sum_{j=1}^l \bar{\gamma}_{l,j} f_j^{\{I\}} + H \sum_{l=1}^i \sum_{j=1}^{l-1} \bar{\omega}_{l,j} f_j^{\{E\}} \\ &= y_n + H \sum_{j=1}^i \left( \sum_{l=j}^i \bar{\gamma}_{l,j} \right) f_j^{\{I\}} + H \sum_{j=1}^{i-1} \left( \sum_{l=j}^i \bar{\omega}_{l,j} \right) f_j^{\{E\}}. \end{aligned}$$

Since the base IMEX-ARK method computes each stage via

$$Y_i^{\{S\}} = y_n + H \sum_{j=1}^i a_{i,j}^{\{I\}} f_j^{\{I\}} + H \sum_{j=1}^{i-1} a_{i,j}^{\{E\}} f_j^{\{E\}}, \quad \text{for } i = 2, \dots, s^{\{S\}},$$

then consistency between the IMEX-MRI and IMEX-ARK methods induces the following conditions on  $\bar{\gamma}_{l,j}$  and  $\bar{\omega}_{l,j}$ :

$$(2.4) \quad \sum_{l=j}^i \bar{\gamma}_{l,j} = a_{i,j}^{\{I\}} \quad \text{and} \quad \sum_{l=1}^i \bar{\omega}_{l,j} = a_{i,j}^{\{E\}} \quad \text{for } i = 2, \dots, s^{\{S\}}.$$

**2.1. Order Conditions.** We derive order conditions for the slow tendency coefficients by first expressing IMEX-MRI methods in GARK form, following similar derivations for other multirate infinitesimal step (MIS)-type methods [3, 30, 34, 38]. To express IMEX-MRI methods in GARK form, we must identify GARK tables  $\mathbf{A}^{\{\sigma,\nu\}}$ ,  $\mathbf{b}^\sigma$  and  $\mathbf{c}^\sigma$  for  $\sigma, \nu \in \{I, E, F\}$ . To this end, we consider the inner fast modified IVP (2.2c) to be evolved using a single step of an arbitrary  $s^{\{F\}}$ -stage Runge–Kutta method with Butcher table  $(A^{\{F,F\}}, b^{\{F\}}, c^{\{F\}})$ , having order of accuracy  $q$  at least as accurate as the IMEX-MRI method. Thus the  $k^{\text{th}}$  fast stage ( $k = 1, \dots, s^{\{F\}}$ ) within the  $i^{\text{th}}$  slow stage ( $i = 2, \dots, s^{\{S\}}$ ) is given by:

$$(2.5) \quad \begin{aligned} Y_k^{\{F,i\}} &= Y_{i-1}^{\{S\}} + H \Delta c_i^{\{S\}} \sum_{l=1}^{s^{\{F\}}} a_{k,l}^{\{F,F\}} f_l^{\{F,i\}} \\ &\quad + H \sum_{j=1}^i \left( \sum_{l=1}^{s^{\{F\}}} a_{k,l}^{\{F,F\}} \gamma_{i,j} \left( c_l^{\{F\}} \right) \right) f_j^{\{I\}} \\ &\quad + H \sum_{j=1}^{i-1} \left( \sum_{l=1}^{s^{\{F\}}} a_{k,l}^{\{F,F\}} \omega_{i,j} \left( c_l^{\{F\}} \right) \right) f_j^{\{E\}}, \end{aligned}$$

where  $f_l^{\{F,i\}} := f^{\{F\}} \left( T_{i-1} + c_l^{\{F\}} \Delta c_i^{\{S\}} H, Y_l^{\{F,i\}} \right)$ . Similarly, the slow stages in this scenario become:

$$(2.6) \quad \begin{aligned} Y_i^{\{S\}} &= Y_{i-1}^{\{S\}} + H \sum_{j=1}^i \left( \sum_{l=1}^{s^{\{F\}}} b_l^{\{F\}} \gamma_{i,j} \left( c_l^{\{F\}} \right) \right) f_j^{\{I\}} \\ &\quad + H \sum_{j=1}^{i-1} \left( \sum_{l=1}^{s^{\{F\}}} b_l^{\{F\}} \omega_{i,j} \left( c_l^{\{F\}} \right) \right) f_j^{\{E\}} \\ &\quad + H \Delta c_i^{\{S\}} \sum_{l=1}^{s^{\{F\}}} b_l^{\{F\}} f_l^{\{F,i\}}. \\ &= y_n + H \sum_{\lambda=1}^i \sum_{j=1}^{\lambda} \left( \sum_{l=1}^{s^{\{F\}}} \sum_{k \geq 0} \gamma_{\lambda,j}^{\{k\}} b_l^{\{F\}} c_l^{\{F\} \times k} \right) f_j^{\{I\}} \\ &\quad + H \sum_{\lambda=1}^i \sum_{j=1}^{\lambda-1} \left( \sum_{l=1}^{s^{\{F\}}} \sum_{k \geq 0} \omega_{\lambda,j}^{\{k\}} b_l^{\{F\}} c_l^{\{F\} \times k} \right) f_j^{\{E\}}, \end{aligned}$$

$$+ H \sum_{\lambda=1}^i \Delta c_{\lambda}^{\{S\}} \sum_{l=1}^{s^{\{F\}}} b_l^{\{F\}} f_l^{\{F,\lambda\}},$$

due to (2.3), and where we use the notation  $c^{\times k}$  to indicate element-wise exponentiation. Using (2.3) again, and our assumption that the fast Runge–Kutta method satisfies  $b^{\{F\}T} c^{\{F\}\times k} = 1/(k+1)$  for  $k = 1, \dots, q$ , we simplify (2.6) to obtain:

$$(2.7) \quad Y_i^{\{S\}} = y_n + H \sum_{j=1}^i \sum_{\lambda=j}^i \bar{\gamma}_{\lambda,j} f_j^{\{I\}} + H \sum_{j=1}^{i-1} \sum_{\lambda=j}^{i-1} \bar{\omega}_{\lambda,j} f_j^{\{E\}} \\ + H \sum_{\lambda=1}^i \sum_{l=1}^{s^{\{F\}}} \Delta c_{\lambda}^{\{S\}} b_l^{\{F\}} f_l^{\{F,\lambda\}}.$$

Recalling that the original IMEX-ARK method had explicit first stage, (2.7) is equivalent to the standard GARK formulation,

$$(2.8) \quad Y_i^{\{S\}} = y_n + H \sum_{j=1}^i a_{i,j}^{\{I,I\}} f_j^{\{I\}} + H \sum_{j=1}^{i-1} a_{i,j}^{\{E,E\}} f_j^{\{E\}} + H \sum_{\lambda=1}^i \sum_{j=1}^{s^{\{F\}}} a_{i,j}^{\{S,F,\lambda\}} f_j^{\{F,\lambda\}},$$

for slow stages  $i = 1, \dots, s^{\{S\}}$ , where we identify the slow-implicit, slow-explicit and slow-fast coupling coefficients as:

$$(2.9) \quad a_{i,j}^{\{I,I\}} := \sum_{\lambda=j}^i \bar{\gamma}_{\lambda,j}, \quad a_{i,j}^{\{E,E\}} := \sum_{\lambda=j}^{i-1} \bar{\omega}_{\lambda,j}, \quad a_{i,j}^{\{S,F,\lambda\}} := \Delta c_{\lambda}^{\{S\}} b_j^{\{F\}}.$$

The first two of these may be represented as the GARK tables

$$(2.10) \quad \mathbf{A}^{\{I,I\}} := E\bar{\Gamma} = A^{\{I,I\}} \quad \text{and} \quad \mathbf{A}^{\{E,E\}} := E\bar{\Omega} = A^{\{E,E\}},$$

where

$$E \in \mathbb{R}^{s^{\{S\}} \times s^{\{S\}}}, \quad E_{i,j} := \begin{cases} 1, & i \geq j, \\ 0, & \text{otherwise.} \end{cases}$$

We note that due to our assumptions on the underlying IMEX-ARK tables,  $\bar{\Gamma}$  is lower-triangular and  $\bar{\Omega}$  is strictly lower-triangular, with both having zero first row.

Furthermore, since the GARK formulation of standard IMEX-ARK methods satisfies  $A^{\{I,E\}} = A^{\{E,E\}}$  and  $A^{\{E,I\}} = A^{\{I,I\}}$  (see [35]), the GARK formulation of our IMEX-MRI method results in the slow-explicit and slow-implicit portions having *shared* slow-fast coupling matrix  $\mathbf{A}^{\{S,F\}} = \mathbf{A}^{\{E,F\}} = \mathbf{A}^{\{I,F\}} \in \mathbb{R}^{s^{\{S\}} \times s}$  with  $s = s^{\{F\}} s^{\{S\}}$ . From (2.9), we have the sub-matrices

$$(2.11) \quad \mathbf{A}^{\{S,F,\lambda\}} := \Delta c_{\lambda}^{\{S\}} \mathbf{g}_{\lambda} b^{\{F\}T}, \quad \text{for } \lambda = 1, \dots, s^{\{S\}},$$

where  $\mathbf{g}_{\lambda} \in \mathbb{R}^{s^{\{S\}}}$  with

$$\left( \mathbf{g}_{\lambda} \right)_i := \begin{cases} 1, & i \geq \lambda, \\ 0, & \text{otherwise.} \end{cases}$$

Combining these into an overall slow-fast coupling matrix, we have

$$(2.12) \quad \mathbf{A}^{\{S,F\}} := \left[ \mathbf{A}^{\{S,F,1\}}, \dots, \mathbf{A}^{\{S,F,s^{\{S\}}\}} \right] = \Delta C^{\{S\}} \otimes b^{\{F\}T},$$

where

$$\Delta C^{\{S\}} := \begin{bmatrix} \Delta c_1^{\{S\}} & 0^{\{F\}T} & \dots & 0^{\{F\}T} \\ \Delta c_1^{\{S\}} & \Delta c_2^{\{S\}} & \dots & 0^{\{F\}T} \\ \vdots & \vdots & \ddots & 0^{\{F\}T} \\ \Delta c_1^{\{S\}} & \Delta c_2^{\{S\}} & \dots & \Delta c_{s^{\{S\}}}^{\{S\}} \end{bmatrix},$$

and  $0^{\{F\}}$  is a column vector of all zeros in  $\mathbb{R}^{s^{\{F\}}}$ .

For completeness, we note the corresponding GARK slow-implicit and slow-explicit coefficients [34],

$$(2.13) \quad \mathbf{b}^{\{I\}} := \mathbb{1}^{\{S\}T} \bar{\Gamma} = b^{\{I\}},$$

$$(2.14) \quad \mathbf{c}^{\{I\}} := E \bar{\Gamma} \mathbb{1}^{\{S\}} = A^{\{I,I\}} \mathbb{1}^{\{S\}} = c^{\{S\}},$$

$$(2.15) \quad \mathbf{b}^{\{E\}} := \mathbb{1}^{\{S\}T} \bar{\Omega} = b^{\{E\}},$$

$$(2.16) \quad \mathbf{c}^{\{E\}} := E \bar{\Omega} \mathbb{1}^{\{S\}} = A^{\{E,E\}} \mathbb{1}^{\{S\}} = c^{\{S\}},$$

where  $\mathbb{1}^{\{S\}} \in \mathbb{R}^{s^{\{S\}}}$  is a column vector of all ones, and we have relied on our assumption of internal consistency in the underlying IMEX-ARK method. From enforcing the row-sum conditions on  $\mathbf{A}^{\{S,F\}}$  we have,

$$(2.17) \quad \mathbf{c}^{\{S,F\}} := \sum_{\lambda=1}^{s^{\{S\}}} \mathbf{A}^{\{S,F,\lambda\}} \mathbb{1}^{\{F\}} = \sum_{\lambda=1}^{s^{\{S\}}} \Delta c_{\lambda} \mathbf{g}_{\lambda}$$

$$\Rightarrow$$

$$\mathbf{c}_i^{\{S,F\}} = \sum_{\lambda=1}^{s^{\{S\}}} (c_{\lambda}^{\{S\}} - c_{\lambda-1}^{\{S\}}) (\mathbf{g}_{\lambda})_i = \sum_{\lambda=1}^i (c_{\lambda}^{\{S\}} - c_{\lambda-1}^{\{S\}}) = c_i^{\{S\}},$$

which ensures internal consistency between each partition of the GARK table (i.e.,  $\mathbf{c}^{\{I,I\}} = \mathbf{c}^{\{E,E\}} = \mathbf{c}^{\{S,F\}} = c^{\{S\}}$ ).

To reveal the GARK coefficients for the fast method and fast-slow couplings, we insert (2.7) into (2.5) to write the  $k^{\text{th}}$  fast stage ( $k = 1, \dots, s^{\{F\}}$ ) within the  $i^{\text{th}}$  slow stage ( $i = 2, \dots, s^{\{S\}}$ ) as:

$$(2.18) \quad Y_k^{\{F,i\}} = y_n + H \sum_{\lambda=1}^{i-1} \sum_{l=1}^{s^{\{F\}}} \Delta c_{\lambda}^{\{S\}} b_l^{\{F\}} f_l^{\{F,\lambda\}} + H \Delta c_i^{\{S\}} \sum_{l=1}^{s^{\{F\}}} a_{k,l}^{\{F,F\}} f_l^{\{F,i\}}$$

$$+ H \sum_{j=1}^{i-1} a_{i-1,j}^{\{I,I\}} f_j^{\{I\}} + H \sum_{j=1}^i \left( \sum_{l=1}^{s^{\{F\}}} a_{k,l}^{\{F,F\}} \gamma_{i,j} (c_l^{\{F\}}) f_j^{\{I\}} \right)$$

$$+ H \sum_{j=1}^{i-2} a_{i-1,j}^{\{E,E\}} f_j^{\{E\}} + H \sum_{j=1}^{i-1} \left( \sum_{l=1}^{s^{\{F\}}} a_{k,l}^{\{F,F\}} \omega_{i,j} (c_l^{\{F\}}) f_j^{\{E\}} \right).$$

The fast method coefficients are therefore:

$$(2.19) \quad \mathbf{A}^{\{F,F\}} := \begin{bmatrix} \Delta c_1^{\{S\}} A^{\{F,F\}} & 0_{s^{\{F\}} \times s^{\{F\}}} & \cdots & 0_{s^{\{F\}} \times s^{\{F\}}} \\ \Delta c_1^{\{S\}} \mathbb{1}^{\{F\}} b^{\{F\}T} & \Delta c_2^{\{S\}} A^{\{F,F\}} & \cdots & \vdots \\ & \Delta c_2^{\{S\}} \mathbb{1}^{\{F\}} b^{\{F\}T} & \cdots & \\ \vdots & \vdots & \ddots & \vdots \\ \Delta c_1^{\{S\}} \mathbb{1}^{\{F\}} b^{\{F\}T} & \Delta c_2^{\{S\}} \mathbb{1}^{\{F\}} b^{\{F\}T} & \cdots & \Delta c_{s^{\{S\}}}^{\{S\}} A^{\{F,F\}} \end{bmatrix}$$

$$= \text{diag}(\Delta c^{\{S\}}) \otimes A^{\{F,F\}} + L \Delta C^{\{S\}} \otimes \mathbb{1}^{\{F\}} b^{\{F\}T} \in \mathbb{R}^{s \times s},$$

where  $\text{diag}(\Delta c^{\{S\}})$  is the diagonal matrix obtained by taking  $\Delta c^{\{S\}}$  as its diagonal entries, and  $L \in \mathbb{R}^{s^{\{S\}} \times s^{\{S\}}}$  with  $L_{i,j} := \delta_{i,j+1}$ . Similarly,

$$(2.20) \quad \mathbf{c}^{\{F\}} := \begin{bmatrix} \Delta c_1^{\{S\}} c^{\{F\}} \\ c_1^{\{S\}} \mathbb{1}^{\{F\}} + \Delta c_2^{\{S\}} c^{\{F\}} \\ \vdots \\ c_{s^{\{S\}}-1}^{\{S\}} \mathbb{1}^{\{F\}} + \Delta c_{s^{\{S\}}}^{\{S\}} c^{\{F\}} \end{bmatrix} = Lc^{\{S\}} \otimes \mathbb{1}^{\{F\}} + \Delta c^{\{S\}} \otimes c^{\{F\}} \in \mathbb{R}^s$$

$$(2.21) \quad \mathbf{b}^{\{F\}} := \begin{bmatrix} \Delta c_1^{\{S\}} b^{\{F\}} \\ \vdots \\ \Delta c_{s^{\{S\}}}^{\{S\}} b^{\{F\}} \end{bmatrix} = \Delta c^{\{S\}} \otimes b^{\{F\}} \in \mathbb{R}^s.$$

Finally, the fast-implicit and fast-explicit coupling coefficients are:

$$(2.22) \quad \mathbf{A}^{\{F,I\}} := \begin{bmatrix} 0_{s^{\{F\}} \times s^{\{S\}}} \\ \mathbb{1}^{\{F\}} (e_1^T A^{\{I,I\}}) + \sum_{k \geq 0} (A^{\{F,F\}} c^{\{F\} \times k}) (e_2^T \Gamma^{\{k\}}) \\ \vdots \\ \mathbb{1}^{\{F\}} (e_{s^{\{S\}}-1}^T A^{\{I,I\}}) + \sum_{k \geq 0} (A^{\{F,F\}} c^{\{F\} \times k}) (e_{s^{\{S\}}}^T \Gamma^{\{k\}}) \end{bmatrix}$$

$$= LA^{\{I,I\}} \otimes \mathbb{1}^{\{F\}} + \sum_{k \geq 0} \Gamma^{\{k\}} \otimes (A^{\{F,F\}} c^{\{F\} \times k}) \in \mathbb{R}^{s \times s^{\{S\}}},$$

$$(2.23) \quad \mathbf{A}^{\{F,E\}} := \begin{bmatrix} 0_{s^{\{F\}} \times s^{\{S\}}} \\ \mathbb{1}^{\{F\}} (e_1^T A^{\{E,E\}}) + \sum_{k \geq 0} (A^{\{F,F\}} c^{\{F\} \times k}) (e_2^T \Omega^{\{k\}}) \\ \vdots \\ \mathbb{1}^{\{F\}} (e_{s^{\{S\}}-1}^T A^{\{E,E\}}) + \sum_{k \geq 0} (A^{\{F,F\}} c^{\{F\} \times k}) (e_{s^{\{S\}}}^T \Omega^{\{k\}}) \end{bmatrix}$$

$$= LA^{\{E,E\}} \otimes \mathbb{1}^{\{F\}} + \sum_{k \geq 0} \Omega^{\{k\}} \otimes (A^{\{F,F\}} c^{\{F\} \times k}) \in \mathbb{R}^{s \times s^{\{S\}}},$$

where we have leveraged the fact that  $\Gamma^{\{k\}}$  and  $\Omega^{\{k\}}$  have zero first row. These give



rise to

$$(2.24) \quad \mathbf{c}^{\{F,I\}} := Lc^{\{S\}} \otimes \mathbb{1}^{\{F\}} + \sum_{k \geq 0} \Gamma^{\{k\}} \mathbb{1}^{\{S\}} \otimes (A^{\{F,F\}} c^{\{F\} \times k}), \quad \text{and}$$

$$(2.25) \quad \mathbf{c}^{\{F,E\}} := Lc^{\{S\}} \otimes \mathbb{1}^{\{F\}} + \sum_{k \geq 0} \Omega^{\{k\}} \mathbb{1}^{\{S\}} \otimes (A^{\{F,F\}} c^{\{F\} \times k}).$$

### 2.1.1. Internal Consistency.

**THEOREM 2.3** (Internal consistency conditions). *IMEX-MRI methods fulfill the “internal consistency” conditions:*

$$(2.26) \quad \mathbf{c}^{\{I,F\}} = \mathbf{c}^{\{E,F\}} = \mathbf{c}^{\{S,F\}} = \mathbf{c}^{\{S\}} \equiv c^{\{S\}},$$

$$(2.27) \quad \mathbf{c}^{\{F,I\}} = \mathbf{c}^{\{F,E\}} = \mathbf{c}^{\{F\}},$$

for any fast method if and only if the following conditions hold:

$$(2.28) \quad \Gamma^{\{0\}} \mathbb{1}^{\{S\}} = \Omega^{\{0\}} \mathbb{1}^{\{S\}} = \Delta c^{\{S\}} \quad \text{and} \quad \Gamma^{\{k\}} \mathbb{1}^{\{S\}} = \Omega^{\{k\}} \mathbb{1}^{\{S\}} = 0 \quad \forall k \geq 1.$$

*Proof.* From the definition of  $\mathbf{c}^{\{S,F\}}$  in equation (2.17), we have already shown that (2.26) satisfied. Now

$$\begin{aligned} \mathbf{c}^{\{F,I\}} = \mathbf{c}^{\{F\}} &\Leftrightarrow \\ Lc^{\{S\}} \otimes \mathbb{1}^{\{F\}} + \sum_{k \geq 0} \Gamma^{\{k\}} \mathbb{1}^{\{S\}} \otimes (A^{\{F,F\}} c^{\{F\} \times k}) &= Lc^{\{S\}} \otimes \mathbb{1}^{\{F\}} + \Delta c^{\{S\}} \otimes c^{\{F\}} \end{aligned}$$

and similarly

$$\begin{aligned} \mathbf{c}^{\{F,E\}} = \mathbf{c}^{\{F\}} &\Leftrightarrow \\ Lc^{\{S\}} \otimes \mathbb{1}^{\{F\}} + \sum_{k \geq 0} \Omega^{\{k\}} \mathbb{1}^{\{S\}} \otimes (A^{\{F,F\}} c^{\{F\} \times k}) &= Lc^{\{S\}} \otimes \mathbb{1}^{\{F\}} + \Delta c^{\{S\}} \otimes c^{\{F\}}, \end{aligned}$$

which are equivalent to the conditions (2.28).  $\square$

**2.1.2. IMEX-MRI Order Conditions.** Due to the structure of the IMEX-MRI method (2.2), many of the GARK order conditions are automatically satisfied. As discussed in [34], since  $\mathbf{A}^{\{I,I\}} = A^{\{I,I\}}$ ,  $\mathbf{A}^{\{E,E\}} = A^{\{E,E\}}$ ,  $\mathbf{b}^{\{I\}} = b^{\{I\}}$ ,  $\mathbf{b}^{\{E\}} = b^{\{E\}}$ ,  $\mathbf{c}^{\{I\}} = c^{\{S\}}$ , and  $\mathbf{c}^{\{E\}} = c^{\{S\}}$  from (2.10) and (2.13)-(2.16), and since our base IMEX-ARK method has order  $q$ , then all of the GARK order conditions up to order  $q$  corresponding to the “slow” components (and their couplings) will be satisfied. Similarly, since ‘infinitesimal’ methods assume that the fast component is solved exactly (or at least using an approximation of order  $\geq q$ ), then the “fast” GARK order  $q$  conditions will similarly be satisfied. Additionally as discussed in [35], if all component tables have order at least two, then an IMEX-MRI method (2.2) that satisfies the internal consistency conditions in Theorem 2.3 will be at least second order accurate. Therefore, in this section we focus on only the remaining coupling conditions between the fast and slow components (both implicit and explicit), for orders three and four.

We make use of the following simplifying conditions as listed in Lemma 3.8 of [34], reproduced here in matrix form, taking into account the structure of our slow base ARK method:

$$(2.29) \quad \mathbf{A}^{\{S,F\}} \mathbf{c}^{\{F\}} = \frac{1}{2} c^{\{S\} \times 2}$$

$$(2.30) \quad \mathbf{b}^{\{I\}T} \mathbf{A}^{\{S,F\}} = \left( (\Delta c^{\{S\}} \times (Db^{\{I\}})) \otimes b^{\{F\}} \right)^T$$

$$(2.31) \quad \mathbf{b}^{\{E\}T} \mathbf{A}^{\{S,F\}} = \left( (\Delta c^{\{S\}} \times (Db^{\{E\}})) \otimes b^{\{F\}} \right)^T$$

$$(2.32) \quad \mathbf{b}^{\{F\}T} \mathbf{A}^{\{F,I\}} = \Delta c^{\{S\}T} \mathcal{A}^{\{I,\zeta\}}$$

$$(2.33) \quad \mathbf{b}^{\{F\}T} \mathbf{A}^{\{F,E\}} = \Delta c^{\{S\}T} \mathcal{A}^{\{E,\zeta\}}$$

$$(2.34) \quad \mathbf{A}^{\{F,I\}} \mathbf{c}^{\{S\}} = \left( (LA^{\{I,I\}}) \otimes \mathbb{1}^{\{F\}} + \sum_{k \geq 0} \Gamma^{\{k\}} \otimes \left( A^{\{F,F\}} c^{\{F\} \times k} \right) \right) c^{\{S\}}$$

$$(2.35) \quad \mathbf{A}^{\{F,E\}} \mathbf{c}^{\{S\}} = \left( (LA^{\{E,E\}}) \otimes \mathbb{1}^{\{F\}} + \sum_{k \geq 0} \Omega^{\{k\}} \otimes \left( A^{\{F,F\}} c^{\{F\} \times k} \right) \right) c^{\{S\}}$$

$$(2.36) \quad \mathbf{A}^{\{F,F\}} \mathbf{c}^{\{F\}} = \frac{1}{2} (Lc^{\{S\}})^{\times 2} \otimes \mathbb{1}^{\{F\}} + \left( (Lc^{\{S\}}) \times \Delta c^{\{S\}} \right) \otimes c^{\{F\}} \\ + \Delta c^{\{S\} \times 2} \otimes \left( A^{\{F,F\}} c^{\{F\}} \right),$$

where we use the notation  $a \times b$  to indicate element-wise multiplication of two vectors, and where we define

$$(2.37) \quad \mathcal{A}^{\{I,\zeta\}} = LA^{\{I,I\}} + \sum_{k \geq 0} \zeta_k \Gamma^{\{k\}}, \quad \mathcal{A}^{\{E,\zeta\}} = LA^{\{E,E\}} + \sum_{k \geq 0} \zeta_k \Omega^{\{k\}},$$

$$L_{i,j} = \delta_{i,j+1}, \quad D_{i,j} = \begin{cases} 1, & j \geq i, \\ 0, & \text{otherwise} \end{cases}$$

and

$$(2.38) \quad \zeta_k = b^{\{F\}T} A^{\{F,F\}} c^{\{F\} \times k} = \frac{1}{(k+1)(k+2)}.$$

**THEOREM 2.4** (Third order conditions). *An internally consistent IMEX-MRI method (2.2) has order three iff the base IMEX-ARK method has order at least three, and the coupling conditions*

$$(2.39) \quad \Delta c^{\{S\}T} \mathcal{A}^{\{I,\zeta\}} c^{\{S\}} = \frac{1}{6} \quad \text{and} \quad \Delta c^{\{S\}T} \mathcal{A}^{\{E,\zeta\}} c^{\{S\}} = \frac{1}{6}$$

hold, where  $\mathcal{A}^{\{I,\zeta\}}$  and  $\mathcal{A}^{\{E,\zeta\}}$  are defined in equation (2.37).

*Proof.* Using (2.29), we have that

$$\mathbf{b}^{\{\sigma\}T} \mathbf{A}^{\{S,F\}} \mathbf{c}^{\{F\}} = \frac{1}{2} b^{\{S\}T} c^{\{S\} \times 2} = \frac{1}{2} \left( \frac{1}{3} \right)$$

for  $\sigma \in \{I, E\}$ , and thus the first two order conditions are automatically satisfied. Similarly, from (2.32) and (2.33) we have

$$\mathbf{b}^{\{F\}T} \mathbf{A}^{\{F,\sigma\}} \mathbf{c}^{\{S\}} = \Delta c^{\{S\}T} \mathcal{A}^{\{\sigma,\zeta\}} c^{\{S\}},$$

which result in the conditions (2.39).  $\square$

**THEOREM 2.5** (Fourth order conditions). *An IMEX-MRI method (2.2) that satisfies Theorem 2.4 has order four iff the base IMEX-ARK method has order at least four, and the following coupling conditions hold for  $\sigma, \nu \in \{I, E\}$ :*

$$(2.40a) \quad \left( \Delta c^{\{S\}} \times Lc^{\{S\}} \right)^T \mathcal{A}^{\{\sigma,\zeta\}} c^{\{S\}} + \left( \Delta c^{\{S\} \times 2} \right)^T \mathcal{A}^{\{\sigma,\beta\}} c^{\{S\}} = \frac{1}{8},$$

$$(2.40b) \quad \Delta c^{\{S\}T} \mathcal{A}^{\{\sigma, \zeta\}} c^{\{S\} \times 2} = \frac{1}{12},$$

$$(2.40c) \quad \left( \Delta c^{\{S\}} \times (Db^{\{\sigma\}}) \right)^T \mathcal{A}^{\{\nu, \zeta\}} c^{\{S\}} = \frac{1}{24},$$

$$(2.40d) \quad \left( \Delta c^{\{S\} \times 2} \right)^T \mathcal{A}^{\{\sigma, \xi\}} c^{\{S\}} + \Delta c^{\{S\}T} L \Delta C^{\{S\}} \mathcal{A}^{\{\sigma, \zeta\}} c^{\{S\}} = \frac{1}{24},$$

$$(2.40e) \quad \Delta c^{\{S\}T} \mathcal{A}^{\{\sigma, \zeta\}} A^{\{\nu, \nu\}} c^{\{S\}} = \frac{1}{24},$$

where we define the auxiliary variables

$$(2.41) \quad \mathcal{A}^{\{I, \beta\}} := \frac{1}{2} LA^{\{I, I\}} + \sum_{k \geq 0} \beta_k \Gamma^{\{k\}}$$

$$(2.42) \quad \mathcal{A}^{\{E, \beta\}} := \frac{1}{2} LA^{\{E, E\}} + \sum_{k \geq 0} \beta_k \Omega^{\{k\}},$$

$$(2.43) \quad \mathcal{A}^{\{I, \xi\}} := \frac{1}{2} LA^{\{I, I\}} + \sum_{k \geq 0} \xi_k \Gamma^{\{k\}},$$

$$(2.44) \quad \mathcal{A}^{\{E, \xi\}} := \frac{1}{2} LA^{\{E, E\}} + \sum_{k \geq 0} \xi_k \Omega^{\{k\}},$$

$$(2.45) \quad \beta_k := (b^{\{F\}} \times c^{\{F\}})^T A^{\{F, F\}} c^{\{F\} \times k} = \frac{1}{(k+1)(k+3)}, \quad \text{and}$$

$$(2.46) \quad \xi_k := b^{\{F\}T} A^{\{F, F\}} A^{\{F, F\}} c^{\{F\} \times k} = \frac{1}{(k+1)(k+2)(k+3)}.$$

*Proof.* Since the GARK representation of our IMEX-MRI method is internally consistent, there are 26 coupling conditions of order 4. Of these, ten are automatically satisfied due the IMEX-MRI method structure and our assumptions on the base IMEX-ARK method, for  $\sigma, \nu \in \{I, E\}$ :

$$(2.47a) \quad \left( \mathbf{b}^{\{\sigma\}} \times \mathbf{c}^{\{S\}} \right)^T \mathbf{A}^{\{S, F\}} \mathbf{c}^{\{F\}} = \frac{1}{8},$$

$$(2.47b) \quad \mathbf{b}^{\{\sigma\}T} \mathbf{A}^{\{\nu, \nu\}} \mathbf{A}^{\{S, F\}} \mathbf{c}^{\{F\}} = \frac{1}{24},$$

$$(2.47c) \quad \mathbf{b}^{\{\sigma\}T} \mathbf{A}^{\{S, F\}} \mathbf{c}^{\{F\} \times 2} = \frac{1}{12},$$

$$(2.47d) \quad \mathbf{b}^{\{\sigma\}T} \mathbf{A}^{\{S, F\}} \mathbf{A}^{\{F, F\}} \mathbf{c}^{\{F\}} = \frac{1}{24}.$$

The remaining 16 order conditions follow from (2.40), for  $\sigma, \nu \in \{I, E\}$ :

$$(2.48a) \quad \left( \mathbf{b}^{\{F\}} \times \mathbf{c}^{\{F\}} \right)^T \mathbf{A}^{\{F, \sigma\}} \mathbf{c}^{\{S\}} = \frac{1}{8},$$

$$(2.48b) \quad \mathbf{b}^{\{F\}T} \mathbf{A}^{\{F, \sigma\}} c^{\{S\} \times 2} = \frac{1}{12},$$

$$(2.48c) \quad \mathbf{b}^{\{\sigma\}T} \mathbf{A}^{\{S, F\}} \mathbf{A}^{\{F, \nu\}} \mathbf{c}^{\{S\}} = \frac{1}{24},$$

$$(2.48d) \quad \mathbf{b}^{\{F\}T} \mathbf{A}^{\{F, F\}} \mathbf{A}^{\{F, \sigma\}} \mathbf{c}^{\{S\}} = \frac{1}{24},$$

$$(2.48e) \quad \mathbf{b}^{\{F\}T} \mathbf{A}^{\{F, \sigma\}} \mathbf{A}^{\{\nu, \nu\}} \mathbf{c}^{\{S\}} = \frac{1}{24},$$

$$(2.48f) \quad \mathbf{b}^{\{F\}T} \mathbf{A}^{\{F,\sigma\}} \mathbf{A}^{\{S,F\}} \mathbf{c}^{\{F\}} = \frac{1}{24}.$$

We first prove the automatically-satisfied conditions (2.47). Using simplifying formula (2.29) and our assumption that the base IMEX-ARK method is order four,

$$\left( \mathbf{b}^{\{\sigma\}} \times \mathbf{c}^{\{S\}} \right)^T \mathbf{A}^{\{S,F\}} \mathbf{c}^{\{F\}} = \frac{1}{2} b^{\{\sigma\}T} c^{\{S\} \times 3} = \frac{1}{2} \left( \frac{1}{4} \right)$$

and

$$\mathbf{b}^{\{\sigma\}T} \mathbf{A}^{\{\nu,\nu\}} \mathbf{A}^{\{S,F\}} \mathbf{c}^{\{F\}} = \frac{1}{2} b^{\{\sigma\}T} A^{\{\nu,\nu\}} c^{\{S\} \times 2} = \frac{1}{2} \left( \frac{1}{12} \right),$$

for  $\sigma, \nu \in \{I, E\}$ , and hence (2.47a) and (2.47b) are satisfied. Using the definition of  $\mathbf{c}^{\{F\}}$  from (2.20), the simplifying formulas (2.30)-(2.31), and our assumptions that  $c_1^{\{S\}} = 0$ , the fast method is at least third order, and the IMEX-ARK method is at least fourth order, we have for  $\sigma \in \{I, E\}$ :

$$\begin{aligned} & \mathbf{b}^{\{\sigma\}T} \mathbf{A}^{\{S,F\}} \mathbf{c}^{\{F\} \times 2} \\ &= \left( (\Delta c^{\{S\}} \times (Db^{\{\sigma\}})) \otimes b^{\{F\}} \right)^T \left( Lc^{\{S\}} \otimes \mathbb{1}^{\{F\}} + \Delta c^{\{S\}} \otimes c^{\{F\}} \right)^{\times 2} \\ &= \left( \Delta c^{\{S\}} \times (Db^{\{\sigma\}}) \right)^T \left( (Lc^{\{S\}})^{\times 2} + (Lc^{\{S\}} \times \Delta c^{\{S\}}) + \frac{1}{3} \Delta c^{\{S\} \times 2} \right) \\ &= \left( Db^{\{\sigma\}} \right)^T \left( (Lc^{\{S\}})^{\times 2} \times \Delta c^{\{S\}} + Lc^{\{S\}} \times \Delta c^{\{S\} \times 2} + \frac{1}{3} \Delta c^{\{S\} \times 3} \right) \\ &= \frac{1}{3} \left( Db^{\{\sigma\}} \right)^T \left( c^{\{S\} \times 3} - (Lc^{\{S\}})^{\times 3} \right) \\ &= \frac{1}{3} \sum_{i=2}^{s^{\{S\}}} \left( \sum_{l=i}^{s^{\{S\}}} b_l^{\{\sigma\}} \right) \left( c_i^{\{S\} \times 3} - c_{i-1}^{\{S\} \times 3} \right) = \frac{1}{3} b^{\{\sigma\}T} c^{\{S\} \times 3} = \frac{1}{3} \left( \frac{1}{4} \right), \end{aligned}$$

which proves the coupling conditions (2.47c). Using the simplifying formulas (2.30), (2.31) and (2.36), and the same assumptions as in the previous step, for  $\sigma \in \{I, E\}$  we have

$$\begin{aligned} & \mathbf{b}^{\{\sigma\}T} \mathbf{A}^{\{S,F\}} \mathbf{A}^{\{F,F\}} \mathbf{c}^{\{F\}} \\ &= \left( (\Delta c^{\{S\}} \times (Db^{\{\sigma\}})) \otimes b^{\{F\}} \right)^T \left( \frac{1}{2} (Lc^{\{S\}})^{\times 2} \otimes \mathbb{1}^{\{F\}} \right. \\ & \quad \left. + \left( (Lc^{\{S\}} \times \Delta c^{\{S\}}) \otimes c^{\{F\}} + \Delta c^{\{S\} \times 2} \otimes (A^{\{F,F\}} c^{\{F\}}) \right) \right) \\ &= \left( \Delta c^{\{S\}} \times (Db^{\{\sigma\}}) \right)^T \left( \frac{1}{2} (Lc^{\{S\}})^{\times 2} + \frac{1}{2} (Lc^{\{S\}} \times \Delta c^{\{S\}}) + \frac{1}{6} \Delta c^{\{S\} \times 2} \right) \\ &= \frac{1}{6} \left( Db^{\{\sigma\}} \right)^T \left( c^{\{S\} \times 3} - (Lc^{\{S\}})^{\times 3} \right) = \frac{1}{6} b^{\{\sigma\}T} c^{\{S\} \times 3} = \frac{1}{6} \left( \frac{1}{4} \right), \end{aligned}$$

and thus the coupling conditions (2.47d) are automatically satisfied as well.

We now examine the 16 remaining fourth-order GARK conditions (2.48). Starting with (2.48a), we use the definitions (2.21) and (2.20), the simplifying formulas (2.34)-

(2.35), and that the fast method is at least second order to obtain:

$$\begin{aligned}
 \frac{1}{8} &= \left( \mathbf{b}^{\{F\}} \times \mathbf{c}^{\{F\}} \right)^T \mathbf{A}^{\{F,I\}} \mathbf{c}^{\{S\}} \\
 &= \left( (\Delta c^{\{S\}} \otimes b^{\{F\}}) \times \left( Lc^{\{S\}} \otimes \mathbb{1}^{\{F\}} + \Delta c^{\{S\}} \otimes c^{\{F\}} \right) \right)^T \\
 &\quad \left( LA^{\{I,I\}} \otimes \mathbb{1}^{\{F\}} + \sum_{k \geq 0} \Gamma^{\{k\}} \otimes \left( A^{\{F,F\}} c^{\{F\} \times k} \right) \right) c^{\{S\}} \\
 &= \left( \Delta c^{\{S\}} \times Lc^{\{S\}} \right)^T \mathcal{A}^{\{I,\zeta\}} c^{\{S\}} + \left( \Delta c^{\{S\} \times 2} \right)^T \mathcal{A}^{\{I,\beta\}} c^{\{S\}}.
 \end{aligned}$$

A similar argument gives

$$\frac{1}{8} = \left( \Delta c^{\{S\}} \times Lc^{\{S\}} \right)^T \mathcal{A}^{\{E,\zeta\}} c^{\{S\}} + \left( \Delta c^{\{S\} \times 2} \right)^T \mathcal{A}^{\{E,\beta\}} c^{\{S\}},$$

which establishes the conditions (2.40a). Using the simplifying formulas (2.32)-(2.33), the order conditions (2.48b) become

$$\frac{1}{12} = \mathbf{b}^{\{F\}T} \mathbf{A}^{\{F,\sigma\}} \mathbf{c}^{\{S\} \times 2} = \Delta c^{\{S\}T} \mathcal{A}^{\{\sigma,\zeta\}} c^{\{S\} \times 2}$$

for  $\sigma \in \{I, E\}$ , which are equivalent to the conditions (2.40b). For the order conditions (2.48c), we use simplifying formulas (2.30)-(2.31) and (2.34) to obtain for  $\sigma \in \{I, E\}$ :

$$\begin{aligned}
 \frac{1}{24} &= \mathbf{b}^{\{\sigma\}T} \mathbf{A}^{\{S,F\}} \mathbf{A}^{\{F,I\}} \mathbf{c}^{\{S\}} \\
 &= \left( (\Delta c^{\{S\}} \times (Db^{\{\sigma\}})) \otimes b^{\{F\}} \right)^T \left( LA^{\{I,I\}} \otimes \mathbb{1}^{\{F\}} + \sum_{k \geq 0} \Gamma^{\{k\}} \otimes \left( A^{\{F,F\}} c^{\{F\} \times k} \right) \right) c^{\{S\}} \\
 &= (\Delta c^{\{S\}} \times (Db^{\{\sigma\}}))^T \mathcal{A}^{\{I,\zeta\}} c^{\{S\}}.
 \end{aligned}$$

Similarly using the simplifying formulas (2.30)-(2.31) and (2.35), we have

$$\frac{1}{24} = (\Delta c^{\{S\}} \times (Db^{\{\sigma\}}))^T \mathcal{A}^{\{E,\zeta\}} c^{\{S\}},$$

resulting in the conditions (2.40c). We use the definitions (2.21) and (2.19), and the simplifying formula (2.34) to convert the order condition (2.48d) for  $\sigma = I$ :

$$\begin{aligned}
 \frac{1}{24} &= \mathbf{b}^{\{F\}T} \mathbf{A}^{\{F,F\}} \mathbf{A}^{\{F,I\}} \mathbf{c}^{\{S\}} \\
 &= \left( \Delta c^{\{S\}} \otimes b^{\{F\}} \right)^T \left( \text{diag} \left( \Delta c^{\{S\}} \right) \otimes A^{\{F,F\}} + L\Delta C^{\{S\}} \otimes \mathbb{1}^{\{F\}} b^{\{F\}T} \right) \\
 &\quad \left( LA^{\{I,I\}} \otimes \mathbb{1}^{\{F\}} + \sum_{k \geq 0} \Gamma^{\{k\}} \otimes \left( A^{\{F,F\}} c^{\{F\} \times k} \right) \right) c^{\{S\}} \\
 &= \left( \left( \Delta c^{\{S\} \times 2} \right)^T \otimes \left( b^{\{F\}T} A^{\{F,F\}} \right) + \Delta c^{\{S\}T} L\Delta C^{\{S\}} \otimes b^{\{F\}T} \right) \\
 &\quad \left( LA^{\{I,I\}} \otimes \mathbb{1}^{\{F\}} + \sum_{k \geq 0} \Gamma^{\{k\}} \otimes \left( A^{\{F,F\}} c^{\{F\} \times k} \right) \right) c^{\{S\}}
 \end{aligned}$$

$$= \left( \Delta c^{\{S\} \times 2} \right)^T \mathcal{A}^{\{I, \xi\}} c^{\{S\}} + \Delta c^{\{S\} T} L \Delta C^{\{S\}} \mathcal{A}^{\{I, \zeta\}} c^{\{S\}}.$$

Similarly, the simplifying formula (2.35) converts (2.48d) for  $\sigma = E$  to

$$\frac{1}{24} = \left( \Delta c^{\{S\} \times 2} \right)^T \mathcal{A}^{\{E, \xi\}} c^{\{S\}} + \Delta c^{\{S\} T} L \Delta C^{\{S\}} \mathcal{A}^{\{E, \zeta\}} c^{\{S\}},$$

which establishes the conditions (2.40d). Using the simplifying formulas (2.32) and (2.33), the order conditions (2.48e) become for  $\sigma, \nu \in \{I, E\}$ :

$$\frac{1}{24} = \mathbf{b}^{\{F\} T} \mathbf{A}^{\{F, \sigma\}} \mathbf{A}^{\{\nu, \nu\}} \mathbf{c}^{\{S\}} = \Delta c^{\{S\} T} \mathcal{A}^{\{\sigma, \zeta\}} \mathcal{A}^{\{\nu, \nu\}} c^{\{S\}},$$

which are the coupling conditions (2.40e). The final order conditions, (2.48f), may be simplified using formulas (2.29) and (2.32)-(2.33) for  $\sigma \in \{I, E\}$ :

$$\frac{1}{24} = \mathbf{b}^{\{F\} T} \mathbf{A}^{\{F, \sigma\}} \mathbf{A}^{\{S, F\}} \mathbf{c}^{\{F\}} = \frac{1}{2} \Delta c^{\{S\}} \mathcal{A}^{\{\sigma, \zeta\}} c^{\{S\} \times 2},$$

which are equivalent to the coupling conditions (2.40b).  $\square$

**3. Linear Stability.** We note that there is no standard theoretical framework for analyzing linear stability of methods for additively-partitioned problems (of *either* form (1.1) or (1.2)). Thus although it relies on an assumption that the Jacobians with respect to  $y$  of  $f^{\{I\}}$ ,  $f^{\{E\}}$  and  $f^{\{F\}}$  are simultaneously diagonalizable, similarly to [34] we analyze linear stability on an additively partitioned scalar test problem:

$$(3.1) \quad y' = \lambda^{\{F\}} y + \lambda^{\{E\}} y + \lambda^{\{I\}} y$$

where each of  $\lambda^{\{F\}}, \lambda^{\{E\}}, \lambda^{\{I\}} \in \mathbb{C}^-$ , and we define  $z^{\{F\}} := H\lambda^{\{F\}}$ ,  $z^{\{E\}} := H\lambda^{\{E\}}$ , and  $z^{\{I\}} := H\lambda^{\{I\}}$ . Applying the IMEX-MRI method (2.2) to the scalar model problem (3.1), the modified fast IVP for each slow stage  $i = 2, \dots, s^{\{S\}}$  becomes:

$$\begin{aligned} v' &= \Delta c_i^{\{S\}} \lambda^{\{F\}} v + \lambda^{\{E\}} \sum_{j=1}^{i-1} \omega_{i,j} \left( \frac{\theta}{H} \right) Y_j^{\{S\}} + \lambda^{\{I\}} \sum_{j=1}^i \gamma_{i,j} \left( \frac{\theta}{H} \right) Y_j^{\{S\}} \\ &= \Delta c_i^{\{S\}} \lambda^{\{F\}} v + \lambda^{\{E\}} \sum_{j=1}^{i-1} \sum_{k \geq 0} \omega_{i,j}^{\{k\}} \frac{\theta^k}{H^k} Y_j^{\{S\}} + \lambda^{\{I\}} \sum_{j=1}^i \sum_{k \geq 0} \gamma_{i,j}^{\{k\}} \frac{\theta^k}{H^k} Y_j^{\{S\}}, \end{aligned}$$

for  $\theta \in [0, H]$ , with initial condition  $v(0) = Y_{i-1}^{\{S\}}$ . We solve for the updated slow stage  $Y_i^{\{S\}} := v(H)$  analytically using the variation of constants formula:

$$\begin{aligned} (3.2) \quad Y_i^{\{S\}} &= e^{\Delta c_i^{\{S\}} z^{\{F\}}} Y_{i-1}^{\{S\}} + z^{\{E\}} \sum_{j=1}^{i-1} \sum_{k \geq 0} \omega_{i,j}^{\{k\}} \left( \int_0^1 e^{\Delta c_i^{\{S\}} z^{\{F\}} (1-t)} t^k dt \right) Y_j^{\{S\}} \\ &\quad + z^{\{I\}} \sum_{j=1}^i \sum_{k \geq 0} \gamma_{i,j}^{\{k\}} \left( \int_0^1 e^{\Delta c_i^{\{S\}} z^{\{F\}} (1-t)} t^k dt \right) Y_j^{\{S\}} \\ &= \varphi_0 \left( \Delta c_i^{\{S\}} z^{\{F\}} \right) Y_{i-1}^{\{S\}} + z^{\{E\}} \sum_{j=1}^{i-1} \eta_{i,j}(z^{\{F\}}) Y_j^{\{S\}} + z^{\{I\}} \sum_{j=1}^i \mu_{i,j}(z^{\{F\}}) Y_j^{\{S\}}, \end{aligned}$$

where  $\eta$  and  $\mu$  depend on the fast variable:

$$\begin{aligned}\eta_{i,j}(z^{\{F\}}) &= \sum_{k \geq 0} \omega_{i,j}^{\{k\}} \varphi_{k+1}(\Delta c_i^{\{S\}} z^{\{F\}}) \\ \mu_{i,j}(z^{\{F\}}) &= \sum_{k \geq 0} \gamma_{i,j}^{\{k\}} \varphi_{k+1}(\Delta c_i^{\{S\}} z^{\{F\}}),\end{aligned}$$

and the family of analytical functions  $\{\varphi_k\}$  are defined as in [34],

$$\varphi_0(z) = e^z, \quad \varphi_k(z) = \int_0^1 e^{z(1-t)} t^k dt, \quad k \geq 1,$$

or recursively as

$$\varphi_{k+1}(z) = \frac{k \varphi_k(z) - 1}{z}, \quad k \geq 1.$$

Concatenating  $Y = \begin{bmatrix} Y_1^{\{S\}T} & \dots & Y_{s\{s\}}^{\{S\}T} \end{bmatrix}^T$ , we can write (3.2) in matrix form as

$$\begin{aligned}Y &= \text{diag}\left(\varphi_0(\Delta c^{\{S\}} z^{\{F\}})\right) LY + \varphi_0(\Delta c_1 z^{\{F\}}) y_n e_1 \\ &\quad + z^{\{E\}} \eta(z^{\{F\}}) Y + z^{\{I\}} \mu(z^{\{F\}}) Y \\ &= \left( I - \text{diag}\left(\varphi_0(\Delta c^{\{S\}} z^{\{F\}})\right) L - z^{\{E\}} \eta(z^{\{F\}}) - z^{\{I\}} \mu(z^{\{F\}}) \right)^{-1} \\ &\quad \varphi_0(\Delta c_1^{\{S\}} z^{\{F\}}) y_n e_1,\end{aligned}$$

where

$$\begin{aligned}\eta(z^{\{F\}}) &= \sum_{k \geq 0} \text{diag}\left(\varphi_{k+1}(\Delta c^{\{S\}} z^{\{F\}})\right) \Omega^{\{k\}} \quad \text{and} \\ \mu(z^{\{F\}}) &= \sum_{k \geq 0} \text{diag}\left(\varphi_{k+1}(\Delta c^{\{S\}} z^{\{F\}})\right) \Gamma^{\{k\}}.\end{aligned}$$

Thus the linear stability function for IMEX-MRI on the problem (3.1) becomes

$$\begin{aligned}(3.3) \quad R(z^{\{F\}}, z^{\{E\}}, z^{\{I\}}) &:= e_{s\{s\}}^T \left( I - \text{diag}\left(\varphi_0(\Delta c^{\{S\}} z^{\{F\}})\right) L - z^{\{E\}} \eta(z^{\{F\}}) - z^{\{I\}} \mu(z^{\{F\}}) \right)^{-1} \\ &\quad \varphi_0(\Delta c_1^{\{S\}} z^{\{F\}}) e_1.\end{aligned}$$

Following a similar definition as in [46], we define the joint stability for the slow, nonstiff region as:

$$\mathcal{J}_{\alpha,\beta} := \left\{ z^{\{E\}} \in \mathbb{C}^- : |R(z^{\{F\}}, z^{\{E\}}, z^{\{I\}})| \leq 1, \quad \forall z^{\{F\}} \in \mathcal{S}_\alpha^{\{F\}}, \quad \forall z^{\{I\}} \in \mathcal{S}_\beta^{\{I\}} \right\}$$

where  $\mathcal{S}_\alpha^\sigma := \{z^\sigma \in \mathbb{C}^- : |\arg(z^\sigma) - \pi| \leq \alpha\}$ . Since such stability regions are not widespread in the literature, we highlight the role of each component, before plotting these for candidate IMEX-MRI methods in the next section. The joint stability region

$\mathcal{J}_{\alpha,\beta}$  provides a plot of the stability region for the slow explicit component only, under assumptions that (a)  $z^{\{I\}}$  can range throughout an entire infinitely-long sector  $\mathcal{S}_\alpha^{\{I\}}$  in the complex left-half plane, and (b)  $z^{\{F\}}$  can range throughout another [infinite] sector  $\mathcal{S}_\beta^{\{F\}}$  in  $\mathbb{C}^-$ . These sectors both include the entire negative real axis, as well as a swath of values with angle at most  $\alpha$  or  $\beta$  above and below this axis, respectively. As such, one should expect the joint stability region  $\mathcal{J}_{\alpha,\beta}$  to be significantly smaller than the standard stability region for just the slow explicit table  $(A^{\{E\}}, b^{\{E\}}, c^{\{E\}})$ , and to shrink in size as both  $\alpha, \beta$  increase. Furthermore, we note that this notion of a joint stability region is artificially restrictive, since in practice the functions  $f^{\{I\}}$  and  $f^{\{F\}}$  will not be *infinitely* stiffer than  $f^{\{E\}}$ .

**4. Example IMEX-MRI Methods.** While our focus in this paper is on the underlying theory regarding IMEX-MRI methods of the form (2.1), in this section we provide some discussion on how IMEX-MRI methods may be constructed, and provide methods of orders 3 and 4 to use in demonstrating our numerical results in Section 5.

**4.1. Third-order Methods.** We create two third order IMEX-MRI methods, both based on the ‘(3,4,3)’ IMEX-ARK method from Section 2.7 of [1],

$$\begin{array}{c|cccc|cccc} 0 & 0 & 0 & 0 & 0 & 0 & 0 & 0 & 0 \\ \eta & \eta & 0 & 0 & 0 & 0 & \eta & 0 & 0 \\ \frac{1+\eta}{2} & a_{3,1} & a_{3,2} & 0 & 0 & 0 & \frac{1-\eta}{2} & \eta & 0 \\ 1 & 1-2\alpha & \alpha & \alpha & 0 & 0 & b_2 & b_3 & \eta \\ \hline 1 & 0 & b_2 & b_3 & \eta & 0 & b_2 & b_3 & \eta \end{array}$$

where

$$\begin{aligned} \eta &= 0.4358665215084589994160194511935568425293, \\ \alpha &= 0.5529291480359398193611887297385924764949, \\ a_{3,2} &= \left(-\frac{15}{4} + 15\eta - \frac{21}{4}\eta^2\right)\alpha + 4 - \frac{25}{2}\eta + \frac{9}{2}\eta^2, \\ a_{3,1} &= \left(\frac{15}{4} - 15\eta + \frac{21}{4}\eta^2\right)\alpha - \frac{7}{2} + 13\eta - \frac{9}{2}\eta^2, \\ b_2 &= -\frac{3}{2}\eta^2 + 4\eta - \frac{1}{4}, \\ b_3 &= \frac{3}{2}\eta^2 - 5\eta + \frac{5}{4}. \end{aligned}$$

As the explicit portion of this pair is not ‘stiffly accurate’ we pad the tables as discussed in Section 2. We then convert this to ‘solve-decoupled’ form [34] by inserting additional rows and columns into the tables to ensure that any stage with a nonzero diagonal value in the slow implicit table is associated with  $\Delta c_i = 0$ ,



0	0	0	0	0	0	0	0	0	0	0	0	0	0	0	0	0	0	0	0
$\eta$	$\eta$	0	0	0	0	0	0	0	0	$\eta$	0	0	0	0	0	0	0	0	0
$\eta$	$\eta$	0	0	0	0	0	0	0	0	0	0	$\eta$	0	0	0	0	0	0	0
$\frac{1+\eta}{2}$	$\square$	0	$\square$	0	0	0	0	0	0	$\square$	0	$\square$	0	0	0	0	0	0	0
$\frac{1+\eta}{2}$	$a_{3,1}$	0	$a_{3,2}$	0	0	0	0	0	0	0	0	$\frac{1-\eta}{2}$	0	$\eta$	0	0	0	0	0
1	$\square$	0	$\square$	0	$\square$	0	0	0	0	$\square$	0	$\square$	0	$\square$	0	0	0	0	0
1	$1 - 2\alpha$	0	$\alpha$	0	$\alpha$	0	0	0	0	0	0	$b_2$	0	$b_3$	0	$\eta$	0	0	0
1	0	0	$b_2$	0	$b_3$	0	$\eta$	0	0	0	0	$b_2$	0	$b_3$	0	$\eta$	0	0	0
1	0	0	$b_2$	0	$b_3$	0	$\eta$	0	0	0	0	$b_2$	0	$b_3$	0	$\eta$	0	0	0
1	0	0	$b_2$	0	$b_3$	0	$\eta$	0	0	0	0	$b_2$	0	$b_3$	0	$\eta$	0	0	0

where each entry in  $A^{\{E,E\}}$  and  $A^{\{I,I\}}$  above labeled with  $\square$  need only be chosen to satisfy internal consistency for the ARK table. We note that although the proposed IMEX-MRI methods (2.2) do not *require* that the implicit portion of the IMEX-ARK table have this ‘solve-decoupled’ pattern, we create tables with this structure due to their ease of implementation. Specifically, if the corresponding IMEX-MRI method included a ‘solve-coupled’ stage  $i$ , i.e., this stage includes both nonzero diagonal value  $\bar{\gamma}_{i,i}$  and nonzero  $\Delta c_i$ , then the stage solution  $Y_i^{\{S\}}$  must *both* define the fast IVP right-hand side (2.2c),

$$v'(\theta) = \Delta c_i^{\{S\}} f^{\{F\}}\left(T_{i-1} + \Delta c_i^{\{S\}}\theta, v(\theta)\right) + \sum_{j=1}^{i-1} \left( \gamma_{i,j}\left(\frac{\theta}{H}\right) f_j^{\{I\}} + \omega_{i,j}\left(\frac{\theta}{H}\right) f_j^{\{E\}} \right) + \gamma_{i,i}\left(\frac{\theta}{H}\right) f^{\{I\}}\left(t_n + c_i^{\{S\}}H, Y_i^{\{S\}}\right), \quad \theta \in [0, H],$$

and be the solution to this fast IVP,  $Y_i^{\{S\}} = v(H)$ . Solve-decoupled methods, on the other hand, may be performed by alternating between standard implicit solves for each implicit stage, followed by fast evolution for non-implicit stages. However, as noted in [29, 30], while the solve-decoupled approach makes for easier implementation of MRI methods, it also results in methods with diminished stability.

Our first IMEX-MRI built from the extended IMEX-ARK table above is “IMEX-MRI3a”. We simultaneously found the 10  $\square$  values to complete the IMEX-ARK table, the 24 unknown  $\Gamma^{\{0\}}$  coefficients and the 20 unknown  $\Omega^{\{0\}}$  coefficients by solving the ARK consistency conditions (2.4), the internal consistency conditions (2.28), and the third order conditions (4.1). Since this only constitutes 50 unique conditions that depend linearly on 54 unknown entries, the corresponding linear system of equations was under-determined. For IMEX-MRI3a we used the particular solution returned by MATLAB (a basic least-squares solution). The resulting nonzero coefficients  $\mathbf{c}^{\{S\}}$ ,  $\Gamma^{\{0\}}$  and  $\Omega^{\{0\}}$  are provided in Appendix A.

Our second IMEX-MRI constructed from this same base IMEX-ARK table is “IMEX-MRI3b”. Here, beginning with the IMEX-MRI3a particular solution above, we then used the four remaining free variables to maximize the extent of the joint stability region along the negative real-axis. The nonzero coefficients  $\mathbf{c}^{\{S\}}$ ,  $\Gamma^{\{0\}}$  and  $\Omega^{\{0\}}$  for the resulting method are given in Appendix B.

*Remark 4.1.* An alternative way of creating solve-decoupled third order IMEX-MRI methods is to take advantage of the free  $\square$  variables within the extended IMEX-ARK table, plus assumptions that  $\bar{\Gamma} = \Gamma^{\{0\}}$  and  $\bar{\Omega} = \Omega^{\{0\}}$ . Here, one may select the  $\square$  values to ensure that the IMEX-ARK is internally consistent and satisfies

$$(4.1) \quad \Delta c^{\{S\}T} \left( L + \frac{1}{2}E^{-1} \right) A^{\{E,E\}} c^{\{S\}} = \frac{1}{6}, \quad \Delta c^{\{S\}T} \left( L + \frac{1}{2}E^{-1} \right) A^{\{I,I\}} c^{\{S\}} = \frac{1}{6},$$

as these are equivalent to the third order coupling conditions (2.39) with equation (2.10) providing one-to-one correspondences between  $A^{\{I,I\}}$  and  $\Gamma^{\{0\}}$ , and between  $A^{\{E,E\}}$  and  $\Omega^{\{0\}}$ . We note that the conditions (4.1) each correspond to the previously-discovered third order condition for MIS methods introduced in [21].

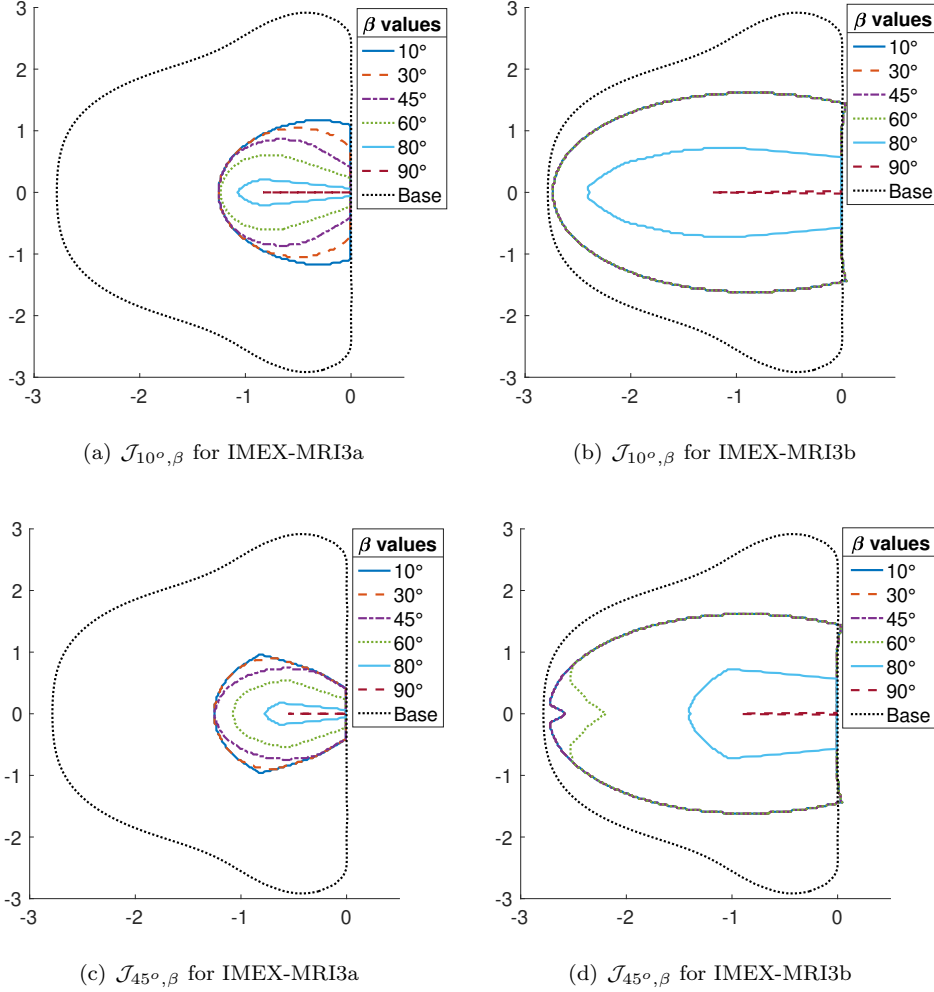


FIG. 1. Joint stability regions  $\mathcal{J}_{\alpha, \beta}$  for both IMEX-MRI3a (left) and IMEX-MRI3b (right), at fast sector angles  $\alpha = 10^\circ$  (top) and  $\alpha = 45^\circ$  (bottom), for a variety of implicit sector angles  $\beta$ . Each plot includes the joint stability region for the base IMEX-ARK table (shown as “Base”). The benefits of simultaneously optimizing the IMEX-MRI coefficients  $\Gamma^{\{0\}}$  and  $\Omega^{\{0\}}$  are clear, as  $\mathcal{J}_{\alpha, \beta}$  for IMEX-MRI3b are significantly larger than those for IMEX-MRI3a.

In Figure 1 we plot the joint stability regions  $\mathcal{J}_{\alpha, \beta}$  for both the IMEX-MRI3a and IMEX-MRI3b methods, for the fast time scale sectors  $\mathcal{S}_\alpha^{\{F\}}$ ,  $\alpha \in \{10^\circ, 45^\circ\}$  and for the slow implicit sectors  $\mathcal{S}_\beta^{\{I\}}$ ,  $\beta \in \{10^\circ, 30^\circ, 45^\circ, 60^\circ, 80^\circ, 90^\circ\}$ . In these figures we also plot the joint stability region for the slow base IMEX-ARK method, taken over implicit slow wedge  $\mathcal{S}_{90^\circ}^{\{I\}}$  (black dotted line). These results indicate that the joint stability regions for IMEX-MRI3a at all fast and implicit sector angles are significantly smaller

than the base IMEX-ARK stability region. Furthermore, these stability regions shrink considerably as the implicit sector angle  $\beta$  grows from  $10^\circ$  to  $80^\circ$ . In contrast, the joint stability regions for IMEX-MRI3b are much larger, encompassing the majority of the base IMEX-ARK stability region for both fast sector angles  $\alpha = 10^\circ$  and  $45^\circ$ , and for implicit sector angles  $\beta \leq 60^\circ$ , including a significant extent along the imaginary axis. We therefore anticipate that this method should provide increased stability for IMEX multirate problems wherein advection comprises the slow explicit portion, as the corresponding Jacobian eigenvalues typically reside on the imaginary axis.

**4.2. Fourth-order Method.** We also constructed a fourth-order IMEX-MRI method using a base IMEX-ARK method of our own design (since we knew of no existing fourth-order method that satisfied the ‘sorted abscissae’ requirement,  $0 \leq c_1^{\{S\}} \leq \dots \leq c_s^{\{S\}} \leq 1$ ). To obtain IMEX-MRI4 we first converted our IMEX-ARK table to solve-decoupled form and then obtained the missing coefficients by satisfying internal consistency of the IMEX-ARK method. We then found the unknowns in  $\Gamma^{\{0\}}$ ,  $\Gamma^{\{1\}}$ ,  $\Omega^{\{0\}}$  and  $\Omega^{\{1\}}$  by solving the linear system resulting from (2.4), (2.28), (2.39) and (2.40) in MATLAB. The nonzero coefficients  $\mathbf{c}^{\{S\}}$ ,  $\Gamma^{\{0\}}$ ,  $\Gamma^{\{1\}}$ ,  $\Omega^{\{0\}}$  and  $\Omega^{\{1\}}$  for this method, again accurate to 36 decimal digits, are given in Appendix C.

While this method indeed satisfies the full set of ARK consistency conditions (2.4), internal consistency conditions (2.28), third order conditions (2.39), and fourth order conditions (2.40), we have not yet been successful at optimizing its joint stability region  $\mathcal{J}_{\alpha,\beta}$ . In fact, even when ignoring the slow-explicit portion by setting  $z^{\{E\}} = 0$  in our stability function (3.3), the implicit+fast joint stability region is very small, rendering the full joint stability regions  $\mathcal{J}_{\alpha,\beta}$  empty. While we have already noted that this definition of joint stability is overly restrictive, and thus there may indeed be applications in which IMEX-MRI4 is suitable, we do not promote its widespread use, but include it here to demonstrate the predicted fourth-order convergence in our multirate example problems.

**5. Numerical Results.** In this section we demonstrate the expected rates of convergence for the IMEX-MRI tables from Section 4. Additionally, we compare the efficiency of the proposed methods against the legacy Lie–Trotter and Strang–Marchuk splittings (1.3) and (1.4). As these results are designed to provide a proof of concept, all computations were performed in MATLAB, and all codes and test problems used in this section are available in the public GitHub repository [8].

**5.1. Kværno-Prothero-Robinson (KPR) Test.** We first consider the KPR test problem adapted from Sandu [34],

$$\begin{bmatrix} u \\ v \end{bmatrix}' = \mathbf{\Pi} \begin{bmatrix} \frac{-3+u^2-\cos(\beta t)}{2u} \\ \frac{-2+v^2-\cos(t)}{2v} \end{bmatrix} - \begin{bmatrix} \frac{\beta \sin(\beta t)}{2u} \\ \frac{\sin(t)}{2v} \end{bmatrix}, \quad t \in \left[0, \frac{5\pi}{2}\right],$$

where

$$\mathbf{\Pi} = \begin{bmatrix} \lambda^{\{F\}} & \frac{1-\varepsilon}{\alpha}(\lambda^{\{F\}} - \lambda^{\{S\}}) \\ -\alpha\varepsilon(\lambda^{\{F\}} - \lambda^{\{S\}}) & \lambda^{\{S\}} \end{bmatrix},$$

and with initial conditions  $u(0) = 2$ ,  $v(0) = \sqrt{3}$ , corresponding to the exact solutions  $u(t) = \sqrt{3 + \cos(\beta t)}$  and  $v(t) = \sqrt{2 + \cos(t)}$ . Here,  $u$  and  $v$  correspond to the ‘fast’ and ‘slow’ solution variables, respectively. We use the parameters  $\lambda^{\{F\}} = -10$ ,  $\lambda^{\{S\}} = -1$ ,  $\varepsilon = 0.1$ ,  $\alpha = 1$ ,  $\beta = 20$ . While this problem does not inherently require

IMEX methods at the slow time scale, it is both nonlinear and non-autonomous, and has an analytical solution. Thus this serves as an excellent problem to assess the convergence rates for the proposed IMEX-MRI methods.

We split this problem into the form (1.2) by setting each portion of the right hand side to be

$$f\{E\} = \begin{bmatrix} 0 \\ \frac{\sin(t)}{2v} \end{bmatrix}, \quad f\{I\} = \begin{bmatrix} 0 & 0 \\ 0 & 1 \end{bmatrix} \mathbf{\Pi} \begin{bmatrix} \frac{-3+u^2-\cos(\beta t)}{2u} \\ \frac{-2+v^2-\cos(t)}{2v} \end{bmatrix}, \quad \text{and}$$

$$f\{F\} = \begin{bmatrix} 1 & 0 \\ 0 & 0 \end{bmatrix} \mathbf{\Pi} \begin{bmatrix} \frac{-3+u^2-\cos \beta t}{2u} \\ \frac{-2+v^2-\cos(t)}{2v} \end{bmatrix} - \begin{bmatrix} \frac{\beta \sin(\beta t)}{2u} \\ 0 \end{bmatrix}.$$

For the fast time scale of each method we use a step of size  $h = \frac{H}{20}$ , where we match the order of the inner solver with the overall method order: IMEX-MRI3 a and b use the third-order explicit ‘‘RK32’’ from equation (233f) of [4], IMEX-MRI4 uses the popular fourth-order explicit ‘‘RK4’’ method from [22], Strang–Marchuk uses the second-order explicit Heun method, and Lie–Trotter uses the explicit forward Euler method. For the implicit slow components of each method we use a standard Newton–Raphson nonlinear solver with dense Jacobian matrix and linear solver.

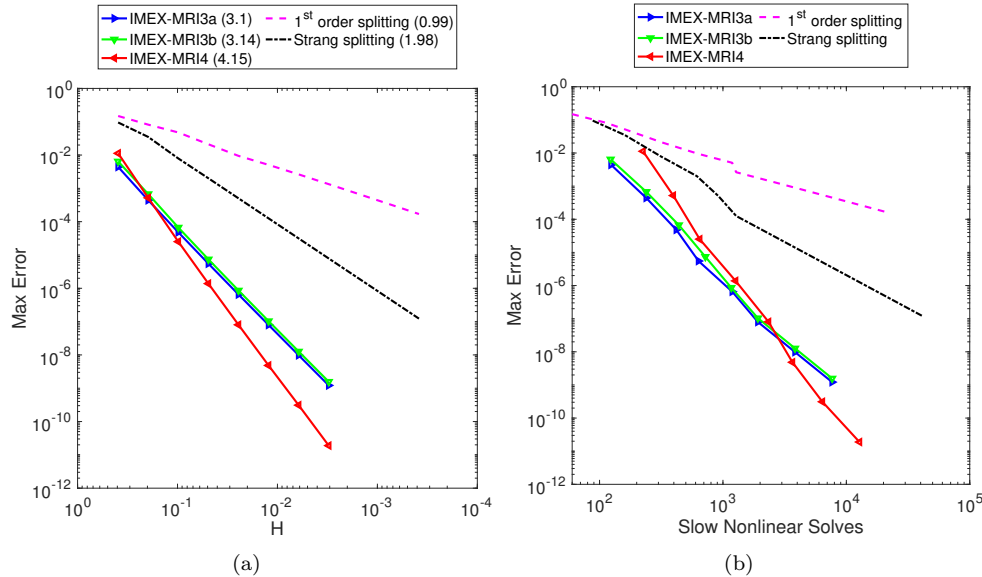


FIG. 2. Convergence (left) and efficiency (right) for the KPR test problem from Section 5.1. The measured convergence rates (given in parentheses) for each method match their theoretical predictions. Measuring ‘efficiency’ as the accuracy vs. the number of implicit solves at the slow time scale, the IMEX-MRI3a and IMEX-MRI3b methods prove most efficient for accuracies larger than around  $10^{-8}$ , while the IMEX-MRI4 method is more efficient at tighter accuracy levels.

In Figure 2 (a) we plot the maximum solution error over a set of 20 evenly-spaced temporal outputs in  $[0, 5\pi/2]$  for each method, at each of the slow step sizes  $H = \pi/2^k$ , for  $k = 3, \dots, 10$  with the IMEX-MRI methods and  $k = 3, \dots, 13$  for the legacy methods. In the legend parentheses we show the overall estimated convergence rate, computed using a least-squares best fit of the  $\log(\text{Max Error})$  versus  $\log(H)$

results for each method. For each method the theoretical order of convergence is reproduced.

Furthermore, assuming that the number of implicit solves at the slow time scale constitutes the dominant cost of each algorithm, we plot the ‘efficiency’ of each method in Figure 2 (b). We note that this measurement accurately accounts for the reduced cost of the simple Lie–Trotter and Strang–Marchuk methods at a given  $H$ . However, even with that benefit, the new IMEX-MRI methods prove considerably more efficient at all accuracy levels, with IMEX-MRI3a and IMEX-MRI3b the most efficient for accuracies above  $10^{-8}$ , and IMEX-MRI4 the most efficient at tighter accuracy levels.

We finally note that the proposed methods enable accuracies that would otherwise be intractable with their legacy counterparts, and that for this problem all methods exhibited comparable stability, robustly computing results at each step size tested.

**5.2. Brusselator Test.** Our second, and more strenuous, test problem focuses on an advection-reaction-diffusion system of partial differential equations, as these are pervasive in computational physics, and are typically solved using one of the two legacy methods (1.3) or (1.4). Here, both advection and diffusion may be evolved at the slow time scale, but due to their differential structure advection is typically treated explicitly, while diffusion is implicit. Chemical reactions, however, frequently evolve on much faster time scales than advection and diffusion, and due to their nonlinearity and bound constraints (typically these are mass densities that must be non-negative), often require subcycling for both accuracy and stability.

We therefore consider the following example which is a stiff variation of the standard “brusselator” test problem [16, 17]:

$$\begin{aligned} u_t &= \alpha_u \nabla^2 u - \rho_u \nabla u + a - (w + 1)u + u^2 v, \\ v_t &= \alpha_v \nabla^2 v - \rho_v \nabla v + wu - u^2 v, \\ w_t &= \alpha_w \nabla^2 w - \rho_w \nabla w + \frac{b - w}{\varepsilon} - wu, \end{aligned}$$

solved on  $t \in [0, 10]$  and  $x \in [0, 1]$ , using stationary boundary conditions,

$$u_t(t, 0) = u_t(t, 1) = v_t(t, 0) = v_t(t, 1) = w_t(t, 0) = w_t(t, 1) = 0,$$

and initial values,

$$\begin{aligned} u(0, x) &= a + 0.1 \sin(\pi x), \\ v(0, x) &= b/a + 0.1 \sin(\pi x), \\ w(0, x) &= b + 0.1 \sin(\pi x), \end{aligned}$$

with parameters  $\alpha_j = 10^{-2}$ ,  $\rho_j = 10^{-3}$ ,  $a = 0.6$ ,  $b = 2$ , and  $\varepsilon = 10^{-2}$ . We discretize these in space using a second order accurate centered difference approximation with 100 grid points. As we do not have an analytical solution to this problem, we compute error by comparing against a reference solution generated using the same spatial grid, but that uses MATLAB’s `ode15s` with an absolute tolerance of  $10^{-14}$  and a relative tolerance of  $2.5e-14$ .

We split this problem into the form (1.2) by setting each portion of the right hand side to be the spatially-discretized versions of the operators

$$f^{\{E\}} = \begin{bmatrix} -\rho_u \nabla u \\ -\rho_v \nabla v \\ -\rho_w \nabla w \end{bmatrix}, \quad f^{\{I\}} = \begin{bmatrix} \alpha_u \nabla^2 u \\ \alpha_v \nabla^2 v \\ \alpha_w \nabla^2 w \end{bmatrix}, \quad \text{and} \quad f^{\{F\}} = \begin{bmatrix} a - (w + 1)u + u^2 v \\ wu - u^2 v \\ \frac{b-w}{\varepsilon} - wu \end{bmatrix}.$$

For the subcycling portions of each method, we use a fast time step of  $h = H/10$ . Again, we use fast implicit methods having accuracy equal to their corresponding multirate method: IMEX-MRI3 a and b use the diagonally-implicit method from Section 3.2.3 of [9] with  $\beta = (3 + \sqrt{3})/6$ , IMEX-MRI4 uses the diagonally-implicit (5,3,4) method from [7], Strang–Marchuk uses the implicit trapezoidal method, and Lie–Trotter uses the implicit Euler method. For both the implicit slow stages and the implicit fast stages we use a standard Newton-Raphson nonlinear solver with sparse Jacobian matrix and linear solver. We note, however, that the fast Jacobians are block-diagonal (one block per finite-difference node), while the slow Jacobians couple unknowns across the entire spatial domain.

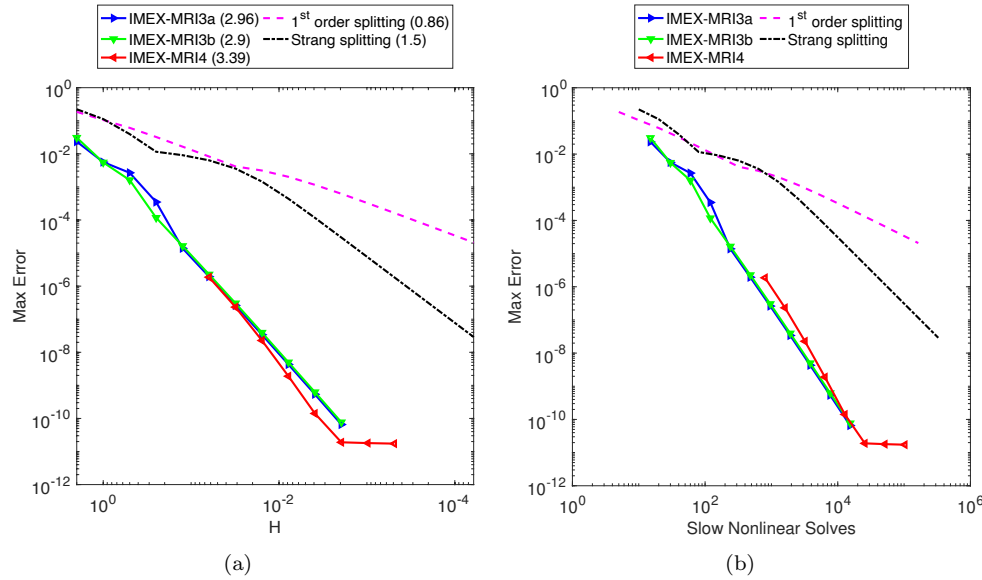


FIG. 3. Convergence (left) and efficiency (right) for the stiff brusselator test problem from Section 5.2. The IMEX-MRI3 methods again demonstrate their theoretical convergence rates, while the other three methods show slight order reduction. The IMEX-MRI3 methods are the most efficient at all accuracy levels, closely followed by IMEX-MRI4. The limited joint stability of the IMEX-MRI4 method is visible, with the red curves missing for  $H > 1/16$ .

In Figure 3 (a) we plot the maximum solution error over a set of 5 evenly-spaced temporal outputs in  $[0, 10]$  for each method, at each of the slow step sizes  $H = 2^{-k}$  for  $k = -1, \dots, 10$  for the third order IMEX-MRI methods,  $k = 8, \dots, 11$  for IMEX-MRI4 and  $k = -1, \dots, 14$  for the legacy methods. We first note that even for this considerably more challenging problem, the ‘lessons’ seen in the previous KPR test problem are largely repeated here. We first note that the IMEX-MRI3 methods again demonstrate near-perfect third order convergence; however the measured convergence rates for IMEX-MRI4, Strang–Marchuk and Lie–Trotter are slightly deteriorated from their theoretical peaks. The reduced convergence for IMEX-MRI4 is likely due to the limited reference solution accuracy of around  $10^{-11}$ , while the reduced convergence rates for the legacy methods result from their poor initial convergence at larger values of  $H$ . Second, we point out that this problem highlights the reduced joint stability region for the IMEX-MRI4 method, as this method was unstable for time step sizes larger than  $H = 1/16$ , while all of the other methods were stable (if inaccurate) at

even the largest step sizes tested.

Finally, again assuming that solution of the implicit stages at the slow time scale dominates the runtime for multirate methods on this problem, we plot the efficiency of each method in Figure 3 (b). As on the KPR problem, the reduced cost per step of the legacy approaches cannot overcome the significant accuracy benefits of the IMEX-MRI methods. However here, we see that the IMEX-MRI3a and IMEX-MRI3b methods prove to be the most efficient at all accuracy levels, with IMEX-MRI4 eventually catching up only at accuracies below  $10^{-10}$ .

**6. Conclusions.** In this paper we have introduced a new class of multirate integration methods that support implicit-explicit treatment of the slow time scale. These IMEX-MRI methods are highly-flexible: in addition to supporting IMEX treatment of the slow time scale, the fast time scale is only assumed to be solved using another sufficiently-accurate approximation, thereby allowing for the fast time scale to be further decomposed into a mix of implicit and explicit components, or even into a multirate method itself. As with their related non-IMEX MRI-GARK counterparts [34], the coupling from slow to fast time scale occurs through modification of the fast time-scale function  $f^{\{F\}}(t, y)$  to include a polynomial forcing term,  $g(t)$ , that incorporates slow-time scale tendencies into the fast time scale dynamics.

In addition to defining IMEX-MRI methods, we have provided rigorous derivation of conditions on their coefficients to guarantee orders three and four. Furthermore, we have provided the corresponding linear stability function for IMEX-MRI methods, and extended Zharovsky et al.’s definition of “joint stability” [46] to accommodate a three-component additive splitting.

With these theoretical foundations, we have presented three specific IMEX-MRI methods, two third order methods derived from Ascher, Ruuth and Spiteri’s ‘(3,4,3)’ ARK method [1], and one fourth order method of our own design. The third order methods exhibit excellent linear stability (particularly IMEX-MRI3b), with stability at least as robust as standard Lie–Trotter and Strang–Marchuk splitting approaches. We then provided asymptotic convergence results for the three proposed methods and the legacy approaches above, using both the oft-utilized Kværno-Prothero-Robinson (KPR) multirate test problem, as well as a more challenging stiff brusselator problem, that is indicative of the multiphysics applications we wish to target. On both of these problems the newly-proposed IMEX-MRI methods exhibit textbook convergence, with efficiencies that far surpass the legacy Lie–Trotter and Strang–Marchuk methods, *particularly* at tighter accuracies.

We note that much work remains. For starters, we would like to derive a new fourth-order IMEX-MRI method with an optimal linear stability region. We anticipate that this will require simultaneous derivatin of both the base IMEX-ARK method *and* its IMEX-MRI extension, due to the tight interplay between these methods and their joint stability. An obvious (yet tedious) extension of this work would be to derive the order conditions for fifth-order IMEX-MRI methods, and to construct tables to implement such approaches. Additionally, we would like to create new IMEX-MRI methods that include embeddings, thereby allowing for robust temporal adaptivity at both the slow and fast time scales. While extension of the IMEX-MRI algorithm to include an alternate set of IMEX-ARK embedding coefficients would be straightforward, creation of optimal embedded multirate methods and fast/slow temporal adaptivity controllers have barely been touched in the literature. Finally, we anticipate the creation of ‘solve-coupled’ IMEX-MRI and MRI-GARK methods, and the associated work on efficient nonlinear solvers, to allow a tighter coupling between

implicit and fast processes in these multirate approaches.

**Acknowledgments.** The authors would like to thank David Gardner, Carol Woodward and John Loffeld for their insightful discussions during the derivation of this work.

### Appendix A. IMEX-MRI3a.

The nonzero coefficients for IMEX-MRI3a (accurate to 36 decimal digits) are:

$$\begin{aligned}
c_1^{\{S\}} &= 0, \\
c_2^{\{S\}} &= c_3^{\{S\}} = 0.4358665215084589994160194511935568425, \\
c_4^{\{S\}} &= c_5^{\{S\}} = 0.7179332607542294997080097255967784213, \\
c_6^{\{S\}} &= c_7^{\{S\}} = c_8^{\{S\}} = c_9^{\{S\}} = 1, \\
\gamma_{2,1}^{\{0\}} &= -\gamma_{3,1}^{\{0\}} = \gamma_{3,3}^{\{0\}} = \gamma_{5,5}^{\{0\}} = \gamma_{6,1}^{\{0\}} = -\gamma_{7,1}^{\{0\}} = \gamma_{7,7}^{\{0\}} \\
&= 0.4358665215084589994160194511935568425, \\
\gamma_{4,1}^{\{0\}} &= -\gamma_{5,1}^{\{0\}} = -0.4103336962288525014599513720161078937, \\
\gamma_{4,3}^{\{0\}} &= 0.6924004354746230017519416464193294724, \\
\gamma_{5,3}^{\{0\}} &= -0.8462002177373115008759708232096647362, \\
\gamma_{6,3}^{\{0\}} &= 0.9264299099302395700444874096601015328, \\
\gamma_{6,5}^{\{0\}} &= -1.080229692192928069168516586450436797, \\
\omega_{2,1}^{\{0\}} &= \omega_{8,7}^{\{0\}} = 0.4358665215084589994160194511935568425, \\
\omega_{4,1}^{\{0\}} &= -0.5688715801234400928465032925317932021, \\
\omega_{4,3}^{\{0\}} &= 0.8509383193692105931384935669350147809, \\
\omega_{5,1}^{\{0\}} &= -\omega_{5,3}^{\{0\}} = 0.454283944643608855878770886900124654, \\
\omega_{6,1}^{\{0\}} &= -0.4271371821005074011706645050390732474, \\
\omega_{6,3}^{\{0\}} &= 0.1562747733103380821014660497037023496, \\
\omega_{6,5}^{\{0\}} &= 0.5529291480359398193611887297385924765, \\
\omega_{8,1}^{\{0\}} &= 0.105858296071879638722377459477184953, \\
\omega_{8,3}^{\{0\}} &= 0.655567501140070250975288954324730635, \\
\omega_{8,5}^{\{0\}} &= -1.197292318720408889113685864995472431.
\end{aligned}$$

### Appendix B. IMEX-MRI3b.

The nonzero coefficients for IMEX-MRI3b (accurate to 36 decimal digits) are:

$$\begin{aligned}
c_1^{\{S\}} &= 0, \\
c_2^{\{S\}} &= c_3^{\{S\}} = 0.4358665215084589994160194511935568425, \\
c_4^{\{S\}} &= c_5^{\{S\}} = 0.7179332607542294997080097255967784213, \\
c_6^{\{S\}} &= c_7^{\{S\}} = c_8^{\{S\}} = c_9^{\{S\}} = 1,
\end{aligned}$$



$$\begin{aligned} \gamma_{2,1}^{\{0\}} &= -\gamma_{3,1}^{\{0\}} = \gamma_{3,3}^{\{0\}} = \gamma_{5,5}^{\{0\}} = \gamma_{7,7}^{\{0\}} \\ &= 0.4358665215084589994160194511935568425, \\ \gamma_{4,1}^{\{0\}} &= -\gamma_{5,1}^{\{0\}} = 0.0414273753564414837153799230278275639, \\ \gamma_{4,3}^{\{0\}} &= 0.2406393638893290165766103513753940148 \\ \gamma_{5,3}^{\{0\}} &= -0.3944391461520175157006395281657292786 \\ \gamma_{6,1}^{\{0\}} &= -\gamma_{7,1}^{\{0\}} = 0.1123373143006047802633543416889605123 \\ \gamma_{6,3}^{\{0\}} &= 1.051807513648115027700693049638099167 \\ \gamma_{6,5}^{\{0\}} &= -0.8820780887029493076720571169238381009 \\ \gamma_{7,3}^{\{0\}} &= -0.1253776037178754576562056399779976346 \\ \gamma_{7,5}^{\{0\}} &= -0.1981516034899787614964594695265986957 \end{aligned}$$

$$\begin{aligned} \omega_{2,1}^{\{0\}} &= \omega_{8,7}^{\{0\}} = 0.4358665215084589994160194511935568425, \\ \omega_{4,1}^{\{0\}} &= -0.1750145285570467590610670000018749059, \\ \omega_{4,3}^{\{0\}} &= 0.4570812678028172593530572744050964846, \\ \omega_{5,1}^{\{0\}} &= -\omega_{5,3}^{\{0\}} = 0.06042689307721552209333459437020635774, \\ \omega_{6,1}^{\{0\}} &= 0.1195213959425454440038786034027936869, \\ \omega_{6,3}^{\{0\}} &= -1.84372522668966191789853395029629765, \\ \omega_{6,5}^{\{0\}} &= 2.006270569992886974186645621296725542, \\ \omega_{7,1}^{\{0\}} &= -0.5466585780430528451745431084418669343, \\ \omega_{7,3}^{\{0\}} &= 2, \\ \omega_{7,5}^{\{0\}} &= -1.453341421956947154825456891558133066, \\ \omega_{8,1}^{\{0\}} &= 0.105858296071879638722377459477184953, \\ \omega_{8,3}^{\{0\}} &= 0.655567501140070250975288954324730635, \\ \omega_{8,5}^{\{0\}} &= -1.197292318720408889113685864995472431. \end{aligned}$$

**Appendix C. IMEX-MRI4.**

The nonzero coefficients for IMEX-MRI4 (accurate to 36 decimal digits) are:

$$\begin{aligned} \mathbf{c}^{\{S\}} &= \left[ 0 \quad \frac{1}{2} \quad \frac{1}{2} \quad \frac{5}{8} \quad \frac{5}{8} \quad \frac{3}{4} \quad \frac{3}{4} \quad \frac{7}{8} \quad \frac{7}{8} \quad 1 \quad 1 \quad 1 \quad 1 \right], \\ \gamma_{2,1}^{\{0\}} &= \frac{1}{2}, \\ \gamma_{3,1}^{\{0\}} &= -\gamma_{3,3}^{\{0\}} = -\gamma_{5,5}^{\{0\}} = -\gamma_{7,7}^{\{0\}} = -\gamma_{9,9}^{\{0\}} = -\gamma_{11,11}^{\{0\}} = -\frac{1}{4}, \\ \gamma_{4,1}^{\{0\}} &= -3.97728124810848818306703385146227889, \\ \gamma_{4,3}^{\{0\}} &= 4.10228124810848818306703385146227889, \\ \gamma_{5,1}^{\{0\}} &= -0.0690538874140169123272414708480937406, \\ \gamma_{5,3}^{\{0\}} &= -0.180946112585983087672758529151906259, \\ \gamma_{6,1}^{\{0\}} &= -1.76176766375792052886337896482241241, \\ \gamma_{6,3}^{\{0\}} &= 2.69452469837729861015533815079146138, \end{aligned}$$

$$\begin{aligned}
\gamma_{6,5}^{\{0\}} &= -0.807757034619378081291959185969048978, \\
\gamma_{7,1}^{\{0\}} &= 0.555872179155396948730508100958808496, \\
\gamma_{7,3}^{\{0\}} &= -0.679914050157999501395850152788348695, \\
\gamma_{7,5}^{\{0\}} &= -\gamma_{8,5}^{\{0\}} = -0.125958128997397447334657948170459801, \\
\gamma_{8,1}^{\{0\}} &= -5.84017602872495595444642665754106511, \\
\gamma_{8,3}^{\{0\}} &= 8.17445668429191508919127080571071637, \\
\gamma_{8,7}^{\{0\}} &= -2.33523878456435658207950209634011106, \\
\gamma_{9,1}^{\{0\}} &= -1.9067926451678118080947593050360523, \\
\gamma_{9,3}^{\{0\}} &= -\gamma_{10,3}^{\{0\}} = -1.54705781138512393363298457924938844 \\
\gamma_{9,5}^{\{0\}} &= -\gamma_{10,5}^{\{0\}} = 4.12988801314935030595449173802031322, \\
\gamma_{9,7}^{\{0\}} &= -\gamma_{10,7}^{\{0\}} = -0.926037556596414564226747853734872477, \\
\gamma_{10,1}^{\{0\}} &= 3.33702815168872605455765278252966252, \\
\gamma_{10,9}^{\{0\}} &= -1.55523550652091424646289347749361021, \\
\gamma_{11,1}^{\{0\}} &= -0.821293629221007618720524112312446752, \\
\gamma_{11,3}^{\{0\}} &= 0.328610356068599988551677264268969646, \\
\gamma_{11,5}^{\{0\}} &= 0.678001812102026694142641232421139516, \\
\gamma_{11,7}^{\{0\}} &= -0.342779287862800022896645471462060708, \\
\gamma_{11,9}^{\{0\}} &= -0.0925392510868190410771489129156017025, \\
\\
\gamma_{4,1}^{\{1\}} &= -\gamma_{4,3}^{\{1\}} = 8.70456249621697636613406770292455778, \\
\gamma_{6,1}^{\{1\}} &= 3.91164310234387488238124087134101229, \\
\gamma_{6,3}^{\{1\}} &= -5.02715717158263104496515924327911025, \\
\gamma_{6,5}^{\{1\}} &= 1.11551406923875616258391837193809796, \\
\gamma_{8,1}^{\{1\}} &= 10.8186076991391180114318371131645132, \\
\gamma_{8,3}^{\{1\}} &= -14.9890852682678311755908413058447354, \\
\gamma_{8,7}^{\{1\}} &= 4.17047756912871316415900419268022213, \\
\gamma_{10,1}^{\{1\}} &= -2.61047101304182849292578695498722043, \\
\gamma_{10,9}^{\{1\}} &= 2.61047101304182849292578695498722043, \\
\\
\omega_{2,1}^{\{0\}} &= \frac{1}{2}, \\
\omega_{4,1}^{\{0\}} &= -1.91716534363662868878172216064946905, \\
\omega_{4,3}^{\{0\}} &= 2.04216534363662868878172216064946905, \\
\omega_{5,1}^{\{0\}} &= -\omega_{5,3}^{\{0\}} = -0.404751031801105942697915907046990469, \\
\omega_{6,1}^{\{0\}} &= 11.4514660224922163666569802860263173, \\
\omega_{6,3}^{\{0\}} &= -30.2107574752650427144064781557395061, \\
\omega_{6,5}^{\{0\}} &= 18.8842914527728263477494978697131888,
\end{aligned}$$

$$\begin{aligned}
 \omega_{7,1}^{\{0\}} &= -0.709033564760261450684711672946330144, \\
 \omega_{7,3}^{\{0\}} &= 1.03030720858751876652616190884004718, \\
 \omega_{7,5}^{\{0\}} &= -\omega_{8,5}^{\{0\}} = -0.321273643827257315841450235893717036, \\
 \omega_{8,1}^{\{0\}} &= -29.9954871645582843984091068494419927, \\
 \omega_{8,3}^{\{0\}} &= 37.605982774991801805364896856243857, \\
 \omega_{8,7}^{\{0\}} &= -7.80676925426077472279724024269558129, \\
 \omega_{9,1}^{\{0\}} &= 3.10466505427296211633876939184912422, \\
 \omega_{9,3}^{\{0\}} &= -\omega_{10,3}^{\{0\}} = -2.43032501975716229713206592741556636, \\
 \omega_{9,5}^{\{0\}} &= -\omega_{10,5}^{\{0\}} = -1.90547930115152463521920165948384213, \\
 \omega_{9,7}^{\{0\}} &= -\omega_{10,7}^{\{0\}} = 1.23113926663572481601249819505028427, \\
 \omega_{10,1}^{\{0\}} &= -2.42442954775204786987587591435551401, \\
 \omega_{10,9}^{\{0\}} &= -0.555235506520914246462893477493610215, \\
 \omega_{11,1}^{\{0\}} &= -0.010441350444797485902945189451653542, \\
 \omega_{11,3}^{\{0\}} &= 0.0726030361465507450515210450548814161, \\
 \omega_{11,5}^{\{0\}} &= -0.128827595167726095223945409857642431, \\
 \omega_{11,7}^{\{0\}} &= 0.112935535009382356613944010712215408, \\
 \omega_{11,9}^{\{0\}} &= \omega_{12,9}^{\{0\}} = -0.0462696255434095205385744564578008512, \\
 \omega_{12,1}^{\{0\}} &= -0.81085227877621013281757892286079321, \\
 \omega_{12,3}^{\{0\}} &= 0.25600731992204924350015621921408823, \\
 \omega_{12,5}^{\{0\}} &= 0.806829407269752789366586642278781947, \\
 \omega_{12,7}^{\{0\}} &= -0.455714822872182379510589482174276116, \\
 \omega_{12,11}^{\{0\}} &= \frac{1}{4} \\
 \\
 \omega_{4,1}^{\{1\}} &= -\omega_{4,3}^{\{1\}} = 4.0843306872732573775634443212989381, \\
 \omega_{6,1}^{\{1\}} &= -21.8434299813822208479181287579586536, \\
 \omega_{6,3}^{\{1\}} &= 59.6120128869278735434171244973850312, \\
 \omega_{6,5}^{\{1\}} &= -37.7685829055456526954989957394263776, \\
 \omega_{8,1}^{\{1\}} &= 61.6590414586370916981876370447766458, \\
 \omega_{8,3}^{\{1\}} &= -77.2725799671586411437821175301678084, \\
 \omega_{8,7}^{\{1\}} &= 15.6135385085215494455944804853911626, \\
 \omega_{10,1}^{\{1\}} &= -\omega_{10,9}^{\{1\}} = -1.11047101304182849292578695498722043.
 \end{aligned}$$

REFERENCES

[1] U. M. ASCHER, S. J. RUUTH, AND R. J. SPITERI, *Implicit-explicit Runge-Kutta methods for time-dependent partial differential equations*, Applied Numerical Mathematics, 25 (1997), pp. 151–167, [https://doi.org/10.1016/S0168-9274\(97\)00056-1](https://doi.org/10.1016/S0168-9274(97)00056-1).

- [2] U. M. ASCHER, S. J. RUUTH, AND B. T. R. WETTON, *Implicit-Explicit Methods for Time-Dependent Partial Differential Equations*, SIAM Journal on Numerical Analysis, 32 (1995), pp. 797–823.
- [3] T. P. BAUER AND O. KNOTH, *Extended multirate infinitesimal step methods: Derivation of order conditions*, Journal of Computational and Applied Mathematics, (2019), p. 112541, <https://doi.org/https://doi.org/10.1016/j.cam.2019.112541>.
- [4] J. C. BUTCHER, *Numerical Methods for Ordinary Differential Equations*, John Wiley & Sons, Apr. 2008.
- [5] A. CARDONE, Z. JACKIEWICZ, A. SANDU, AND H. ZHANG, *Extrapolation-based implicit-explicit general linear methods*, Numer. Algor., 65 (2014), pp. 377–399, <https://doi.org/10.1007/s11075-013-9759-y>.
- [6] A. CARDONE, Z. A. JACKIEWICZ, A. SANDU, AND H. ZHANG, *Construction of highly stable implicit-explicit general linear methods*, Conference Publications, 2015 (2015), p. 185, <https://doi.org/10.3934/proc.2015.0185>.
- [7] J. R. CASH, *Diagonally Implicit Runge-Kutta Formulae with Error Estimates*, IMA J Appl Math, 24 (1979), pp. 293–301, <https://doi.org/10.1093/imamat/24.3.293>.
- [8] R. CHINOMONA AND D. R. REYNOLDS, *Implicit-Explicit Multirate Infinitesimal (IMEX-MRI) Methods*. <https://github.com/rujekoc/imexmri>, 2020.
- [9] S. CONDE, S. GOTTLIEB, Z. J. GRANT, AND J. N. SHADID, *Implicit and Implicit-Explicit Strong Stability Preserving Runge-Kutta Methods with High Linear Order*, J Sci Comput, 73 (2017), pp. 667–690, <https://doi.org/10.1007/s10915-017-0560-2>.
- [10] E. M. CONSTANTINESCU AND A. SANDU, *Extrapolated Multirate Methods for Differential Equations with Multiple Time Scales*, J Sci Comput, 56 (2013), pp. 28–44, <https://doi.org/10.1007/s10915-012-9662-z>.
- [11] G. J. COOPER AND A. SAYFY, *Additive Methods for the Numerical Solution of Ordinary Differential Equations*, Math. Comp., 35 (1980), pp. 1159–1172.
- [12] G. J. COOPER AND A. SAYFY, *Additive Runge-Kutta methods for stiff ordinary differential equations*, Math. Comp., 40 (1983), pp. 207–207, <https://doi.org/10.1090/S0025-5718-1983-0679441-1>.
- [13] D. ESTEP, V. GINTING, D. ROPP, J. N. SHADID, AND S. TAVENER, *An A Posteriori–A Priori Analysis of Multiscale Operator Splitting*, SIAM J. Numer. Anal., 46 (2008), pp. 1116–1146, <https://doi.org/10.1137/07068237X>.
- [14] C. W. GEAR AND D. R. WELLS, *Multirate linear multistep methods*, BIT, 24 (1984), pp. 484–502, <https://doi.org/10.1007/BF01934907>.
- [15] M. GÜNTHER AND A. SANDU, *Multirate generalized additive Runge Kutta methods*, Numer. Math., 133 (2016), pp. 497–524, <https://doi.org/10.1007/s00211-015-0756-z>.
- [16] E. HAIRER, S. P. NØRSETT, AND G. WANNER, *Solving Ordinary Differential Equations I: Nonstiff Problems*, Springer Series in Computational Mathematics, Springer-Verlag, Berlin Heidelberg, second ed., 1993, <https://doi.org/10.1007/978-3-540-78862-1>.
- [17] E. HAIRER AND G. WANNER, *Solving Ordinary Differential Equations II: Stiff and Differential-Algebraic Problems*, Springer Series in Computational Mathematics, Springer-Verlag, Berlin Heidelberg, second ed., 1996, <https://doi.org/10.1007/978-3-642-05221-7>.
- [18] M. HOCHBRUCK AND A. OSTERMANN, *Explicit Exponential Runge-Kutta Methods for Semilinear Parabolic Problems*, SIAM J. Numer. Anal., 43 (2005), pp. 1069–1090, <https://doi.org/10.1137/040611434>.
- [19] C. A. KENNEDY AND M. H. CARPENTER, *Additive Runge-Kutta schemes for convection-diffusion-reaction equations*, Applied Numerical Mathematics, 44 (2003), pp. 139–181, [https://doi.org/10.1016/S0168-9274\(02\)00138-1](https://doi.org/10.1016/S0168-9274(02)00138-1).
- [20] C. A. KENNEDY AND M. H. CARPENTER, *Higher-order additive Runge-Kutta schemes for ordinary differential equations*, Applied Numerical Mathematics, 136 (2019), pp. 183–205, <https://doi.org/10.1016/j.apnum.2018.10.007>.
- [21] O. KNOTH AND R. WOLKE, *Implicit-explicit runge-kutta methods for computing atmospheric reactive flows*, Applied Numerical Mathematics, 28 (1998), pp. 327 – 341, [https://doi.org/10.1016/S0168-9274\(98\)00051-8](https://doi.org/10.1016/S0168-9274(98)00051-8).
- [22] W. KUTTA, *Beitrag zur näherungsweise integration totaler differentialgleichungen*, Zeitschrift für Math. u. Phys., 46 (1901), pp. 435–453.
- [23] V. T. LUAN, R. CHINOMONA, AND D. R. REYNOLDS, *A New Class of High-Order Methods for Multirate Differential Equations*, SIAM Journal on Scientific Computing, 42 (2020), pp. A1245–A1268, <https://doi.org/10.1137/19M125621X>.
- [24] V. T. LUAN AND A. OSTERMANN, *Explicit exponential Runge-Kutta methods of high order for parabolic problems*, Journal of Computational and Applied Mathematics, 256 (2014), pp. 168–179, <https://doi.org/10.1016/j.cam.2013.07.027>.

- [25] V. T. LUAN AND A. OSTERMANN, *Exponential Rosenbrock methods of order five — construction, analysis and numerical comparisons*, Journal of Computational and Applied Mathematics, 255 (2014), pp. 417–431, <https://doi.org/10.1016/j.cam.2013.04.041>.
- [26] G. I. MARCHUK, *Some application of splitting-up methods to the solution of mathematical physics problems*, Aplikace Matematiky, 13 (1968), pp. 103–132, <http://eudml.org/doc/14518>.
- [27] R. I. MCLACHLAN AND G. R. W. QUISPEL, *Splitting methods*, Acta Numerica, 11 (2002), pp. 341–434, <https://doi.org/10.1017/S0962492902000053>.
- [28] G. RAINWATER AND M. TOKMAN, *A new class of split exponential propagation iterative methods of Runge–Kutta type (sEPIRK) for semilinear systems of ODEs*, Journal of Computational Physics, 269 (2014), pp. 40–60, <https://doi.org/10.1016/j.jcp.2014.03.012>.
- [29] S. ROBERTS, J. LOFFELD, A. SARSHAR, C. S. WOODWARD, AND A. SANDU, *Implicit multirate GARK methods*, arXiv:1910.14079 [cs, math], (2019), <https://arxiv.org/abs/1910.14079>.
- [30] S. ROBERTS, A. SARSHAR, AND A. SANDU, *Coupled Multirate Infinitesimal GARK Schemes for Stiff Systems with Multiple Time Scales*, arXiv:1812.00808 [cs, math], (2020), <https://arxiv.org/abs/1812.00808>.
- [31] S. ROBERTS, A. SARSHAR, AND A. SANDU, *Parallel implicit-explicit general linear methods*, arXiv:2002.00868 [cs, math], (2020), <https://arxiv.org/abs/2002.00868>.
- [32] D. L. ROPP AND J. N. SHADID, *Stability of operator splitting methods for systems with indefinite operators: Reaction-diffusion systems*, Journal of Computational Physics, 203 (2005), pp. 449–466, <https://doi.org/10.1016/j.jcp.2004.09.004>.
- [33] A. SANDU, *A Class of Multirate Infinitesimal GARK Methods*, SIAM J. Numer. Anal., 57 (2019), pp. 2300–2327, <https://doi.org/10.1137/18M1205492>.
- [34] A. SANDU, *A Class of Multirate Infinitesimal GARK Methods*, SIAM Journal on Numerical Analysis, 57 (2019), pp. 2300–2327, <https://doi.org/10.1137/18M1205492>.
- [35] A. SANDU AND M. GÜNTHER, *A Generalized-Structure Approach to Additive Runge–Kutta Methods*, SIAM J. Numer. Anal., 53 (2015), pp. 17–42, <https://doi.org/10.1137/130943224>.
- [36] M. SCHLEGEL, O. KNOTH, M. ARNOLD, AND R. WOLKE, *Multirate Runge–Kutta schemes for advection equations*, Journal of Computational and Applied Mathematics, 226 (2009), pp. 345–357, <https://doi.org/10.1016/j.cam.2008.08.009>.
- [37] M. SCHLEGEL, O. KNOTH, M. ARNOLD, AND R. WOLKE, *Numerical solution of multiscale problems in atmospheric modeling*, Appl. Numer. Math., 62 (2012), pp. 1531–1543, <https://doi.org/10.1016/j.apnum.2012.06.023>.
- [38] J. M. SEXTON AND D. R. REYNOLDS, *Relaxed multirate infinitesimal step methods*, 2018, <https://arxiv.org/abs/1808.03718>.
- [39] J. M. SEXTON AND D. R. REYNOLDS, *Relaxed Multirate Infinitesimal Step Methods for Initial-Value Problems*, arXiv:1808.03718 [cs, math], (2019), <https://arxiv.org/abs/1808.03718>.
- [40] G. STRANG, *On the Construction and Comparison of Difference Schemes*, SIAM J. Numer. Anal., 5 (1968), pp. 506–517, <https://doi.org/10.1137/0705041>.
- [41] M. TOKMAN, *A new class of exponential propagation iterative methods of Runge–Kutta type (EPIRK)*, Journal of Computational Physics, 230 (2011), pp. 8762–8778, <https://doi.org/10.1016/j.jcp.2011.08.023>.
- [42] M. TOKMAN, J. LOFFELD, AND P. TRANQUILLI, *New Adaptive Exponential Propagation Iterative Methods of Runge–Kutta Type*, SIAM J. Sci. Comput., 34 (2012), pp. A2650–A2669, <https://doi.org/10.1137/110849961>.
- [43] J. WENSCH, O. KNOTH, AND A. GALANT, *Multirate infinitesimal step methods for atmospheric flow simulation*, Bit Numer Math, 49 (2009), pp. 449–473, <https://doi.org/10.1007/s10543-009-0222-3>.
- [44] H. ZHANG, A. SANDU, AND S. BLAISE, *Partitioned and Implicit–Explicit General Linear Methods for Ordinary Differential Equations*, J Sci Comput, 61 (2014), pp. 119–144, <https://doi.org/10.1007/s10915-014-9819-z>.
- [45] H. ZHANG, A. SANDU, AND S. BLAISE, *High Order Implicit-explicit General Linear Methods with Optimized Stability Regions*, SIAM J. Sci. Comput., 38 (2016), pp. A1430–A1453, <https://doi.org/10.1137/15M1018897>.
- [46] E. ZHAROVSKY, A. SANDU, AND H. ZHANG, *A class of implicit-explicit two-step runge–kutta methods*, SIAM Journal on Numerical Analysis, 53 (2015), pp. 321–341, <https://doi.org/10.1137/130937883>.